doi:10.26443/seismica.v5i1.2065

Activating a Natural Fault Zone in the Swiss Alps

Men-Andrin Meier [*1,2], **Paul A Selvadurai** [2], **Valentin Gischig** [10], **Marian Hertrich** [1], **Elisa Tinti** [5], **Antonio Pio Rinaldi** [2], **Mohammedreza Jalali** [4], **Elena Spagnuolo** [3], **Alba Zappone** [2], **Luca Dal Zilio** [12], **Giacomo Pozzi** [8], **Frédérick Massin** [2], **Alberto Ceccato** [1], **Alexis Shakas** [1], **Peter Achtziger-Zupančič** [7], **Stefano Aretusini** [3], **Viola Becattini** [2], **Kathrin Behnen** [1], **Kai Bröker** [11], **Victor Classen Repollés** [1], **John Clinton** [2], **Cristiano Collettini** [5], **Paul Cook**[9], **Chiara Cornelio** [3], **Georgia Cua**[1], **Nikolaj Dahmen** [2], **Jonas Dickmann** [4], **Fiona Dresler-Dorn** [1], **Virginie Durand** [13], **Pascal Edme** [2], **Nima Gholizadeh Doonechaly** [1], **Guiseppe Volpe** [5], **Yves Guglielmi** [9], **Ivo Graber**[1], **Thomas Haag** [1], **Leon Hibbard** [2], **Rebecca Hochreutener** [1], **Danyang Jiang** [2], **Philipp Kästli** [2], **Barnabas Kövér** [1], **Michal Kruszewski** [4], **Aurora Lambiase** [2], **Federica Lanza** [2], **Laura Laurenti** [2], **Alexandra Lightfoot** [2], **Cara Magnabosco** [10], **Michèle Marti** [2], **Hansruedi Maurer** [1], **Olivier Meyers** [1], **Leila Mizrahi** [2], **Francesco Mosconi** [5], **Anne Obermann** [2], **Kadek Palgunadi** [2], **Edoardo Pezzulli** [2], **Katrin Plenkers** [6], **Giulio Poggiali** [5], **Pooya Hamdi** [4], **Martina Rosskopf** [1], **Luca Scarabello** [1], **Tom Schaber** [4], **Nico Schliwa** [1], **Ryan Schultz** [2], **Miriam Schwarz** [2], **Florian Soom** [9], **Mariano Supino** [3], **Lu Tian** [1], **Katinka Tuinstra** [2], **Liliana Vargas-Meleza** [1], **Linus Villgier** [2], **Zhe Wang** [10], **Mathilde Wimez** [1], **Jiayi Ye** [1], **Stefanie Zeller**[2], **Eric Zimmermann**[2], **Florian Amann** [4], **Massimo Cocco** [3], **Stefan Wiemer** [2], **Domenico Giardini** [1]

[1]Institute of Geophysics, ETH Zurich, Zurich, Switzerland, [2]Swiss Seismological Service, ETH Zurich, Zurich, Switzerland, [3]Instituto Nazionale di Geofisica e Vulcanologia, Rome, Italy, [4]RWTH University of Aachen, Aachen, Germany, [5]Sapienza University of Rome, Rome, Italy, [6]GMuG GmbH, Dieselstr. 9, 61231 Bad Nauheim, Germany, [7]Fraunhofer IEG, Fraunhofer Research Institution for Energy Infrastructures and Geotechnologies IEG, Aachen, [8]Department of Geosciences, University of Padua, Padova, Italy, [9]Lawrence Berkeley National Laboratory (LBNL), Berkeley, CA, USA, [10]Geological Institute, ETH Zurich, Zurich, Switzerland, [11]Center for Hydrogeology and Geothermics, University of Neuchâtel, Neuchâtel, Switzerland, [12]Nanyang Technological University, Singapore, [13]Laboratoire GéoAzur, Université Côte d'Azur, Nice, France

Author contributions: *Conceptualization*: F Amann, M Cocco, L Dal Zilio, D Giardini, V Gischig, M Hertrich, M Jalali, H Maurer, M Meier, A Rinaldi, P Selvadurai, E Tinti, S Wiemer. *Data curation*: P Achtziger-Zupančič, K Behnen, A Ceccato, I Graber, T Haag, M Hertrich, F Massin, M Meier, G Pozzi, A Rinaldi, L Scarabello, P Selvadurai, A Shakas, E Spagnuolo, L Vargas-Meleza, G Volpe, Z Wang. *Formal analysis*: P Achtziger-Zupančič, A Ceccato, V Classen Repollés, J Clinton, P Cook, C Cornelio, N Dahmen, J Dickmann, V Durand, P Edme, N Gholizadeh Doonechaly, Y Guglielmi, T Haag, P Hamdi, M Hertrich, M Jalali, B Kövér, M Kruszewski, A Lambiase, L Laurenti, A Lightfoot, F Massin, H Maurer, M Meier, O Meyers, L Mizrahi, F Mosconi, K Palgunadi, G Pozzi, A Rinaldi, M Rosskopf, T Schaber, N Schliwa, M Schwarz, P Selvadurai, A Shakas, F Soom, M Supino, L Tian, E Tinti, K Tuinstra, L Villgier. *Funding aquisition*: F Amann, M Cocco, D Giardini, M Hertrich, M Meier, A Obermann, A Rinaldi, E Tinti, S Wiemer, J Ye. *Investigation*: P Achtziger-Zupančič, F Amann, S Aretusini, K Bröker, A Ceccato, J Clinton, M Cocco, C Collettini, N Dahmen, L Dal Zilio, D Giardini, V Gischig, T Haag, M Jalali, A Lambiase, C Magnabosco, F Massin, M Meier, F Mosconi, K Palgunadi, K Plenkers, E Pezzulli, G Pozzi, G Poggiali, A Rinaldi, M Rosskopf, T Schaber, P Selvadurai, A Shakas, F Soom, E Spagnuolo, M Supino, L Tian, E Tinti, K Tuinstra, G Volpe, Z Wang, S Wiemer, A Zappone, E Zimmermann. *Methodology*: P Achtziger-Zupančič, S Aretusini, A Ceccato, L Dal Zilio, V Gischig, M Hertrich, M Jalali, P Kästli, F Massin, M Meier, L Mizrahi, G Pozzi, A Rinaldi, P Selvadurai, E Spagnuolo, M Supino, E Tinti, L Villgier, G Volpe. *Project administration*: F Amann, V Becattini, J Clinton, M Cocco, G Cua, D Giardini, M Hertrich, R Hochreutener, R Hochreutener, M Jalali, F Lanza, M Marti, M Meier, E Tinti, S Wiemer, M Wimez. *Resources*: Y Guglielmi, M Hertrich, R Hochreutener, R Hochreutener, M Jalali, P Kästli, M Meier, A Rinaldi, A Shakas, E Tinti, L Vargas-Meleza, M Wimez. *Software*: T Haag, P Kästli, F Massin, A Rinaldi, L Scarabello, A Shakas, M Supino. *Supervision*: F Amann, J Clinton, M Cocco, D Giardini, Y Guglielmi, M Hertrich, M Jalali, C Magnabosco, H Maurer, M Meier, A Rinaldi, P Selvadurai, A Shakas, E Tinti, S Wiemer, M Wimez. *Validation*: A Lightfoot, F Massin, M Meier, A Rinaldi, P Selvadurai. *Visualization* : A Ceccato, P Hamdi, M Hertrich, F Massin, M Meier, G Pozzi, A Rinaldi, P Selvadurai, A Shakas, L Tian, A Zappone, S Zeller. *Writing – original draft*: F Amann, M Cocco, D Giardini, M Meier, P Selvadurai, S Wiemer. *Writing – review & editing*: P Achtziger-Zupančič, F Amann, S Aretusini, K Behnen, K Bröker, A Ceccato, V Classen Repollés, M Cocco, L Dal Zilio, F Dresler-Dorn, D Giardini, V Gischig, P Hamdi, M Hertrich, L Hibbard, D Jiang, P Kästli, L Laurenti, A Lightfoot, C Magnabosco, F Massin, M Meier, L Mizrahi, A Obermann, K Palgunadi, K Plenkers, E Pezzulli, G Pozzi, G Poggiali, A Rinaldi, M Rosskopf, R Schultz, M Schwarz, P Selvadurai, E Spagnuolo, M Supino, L Tian, E Tinti, K Tuinstra, L Vargas-Meleza, L Villgier, Z Wang, S Wiemer, M Wimez, A Zappone.

Abstract One major hurdle for understanding earthquake mechanics are observational limitations. Important phenomena like strain localisation, fault dilation, and fault healing are readily studied in rock mechanical laboratory experiments and with numerical models. At the scale of natural earthquakes, however, these phenomena are often unresolvable, even by state-of-the-art observatories. To overcome this limitation, we are currently building the Earthquake Physics Testbed at the Bedretto Underground Laboratory for Geosciences and Geoenergies (BedrettoLab), an experimental testbed where we can activate an extensively instrumented natural fault zone via hydraulic stimulation. The goal of the Fault Activation and Earthquake Rupture (FEAR) project is to induce earthquakes of up to M_w~1.0 on this exceptionally well characterised and instrumented fault zone. Here we summarize the main scientific goals and current FEAR project status, and present first results from conducted experiments. We discuss how this large-scale experimental approach may allow us to tackle both fundamental science as well as practical questions on earthquake physics, induced seismicity and seismic hazard.

Production Editor: Gareth Funning
Handling Editor: Ake Fagereng
Copy & Layout Editor: Hannah F. Mark

Signed reviewer(s): John Vidale

Received: October 10, 2025
Accepted: January 12, 2026
Published: February 12, 2026

*Corresponding author: menandrin.meier@eaps.ethz.ch

Non-technical summary A major challenge in earthquake science is that many key processes are difficult to observe directly in nature. Laboratory experiments and numerical models can reproduce phenomena such as subtle and slow rock deformation before and after major events, but these remain nearly unresolvable during real earthquakes. In the framework of the Fault Activation and Earthquake Rupture (FEAR) project, we are building a unique experimentation facility at the Bedretto Underground Laboratory for Geosciences and Geoenergies (BedrettoLab) in Switzerland, where we are instrumenting a natural fault zone with a wide range of monitoring equipment and an experiment control system. With fluid injections into the fault zone, we aim to induce fault deformation and associated processes, and to trigger earthquakes with target magnitudes of up to magnitude 1.0. This setup should allow us to directly measure fault processes in unprecedented detail, and to advance our understanding of both earthquake mechanics and practical aspects of induced seismicity.

1 Introduction

Understanding the physics of earthquakes is challenging, because of the complexity of earthquake phenomena and because it is difficult to observe fault processes in situ. As of today, many fundamental questions about the seismic cycle remain unanswered, from fault zone preparation; to dynamic rupture nucleation, propagation, and arrest; to post-seismic and off-fault processes. Our limited understanding of fault zone mechanics is not only a scientific frontier but also a major obstacle for developing more effective earthquake risk mitigation tools, and for our ability to anticipate, forecast, and possibly even predict future large earthquakes (Grigoli et al., 2018; Moein et al., 2023).

Faults exhibit a range of deformation modes, from seismic (fast) to aseismic (slow) modes, including slow slip events (Beroza and Ide, 2011; Dragert et al., 2001; Ide et al., 2007), tremors (Obara, 2002), and low and very low-frequency events (Ito et al., 2007). As tectonic stresses approach a faults' strength, it experiences sub-critical damage and volumetric weakening processes, leading to earthquakes (Kato and Ben-Zion, 2021). The underlying physical and chemical processes span a wide range of spatial and temporal scales (Ben-Zion, 2008) and can interact through various feedback mechanisms. These processes occur within fault zones that are structurally heterogeneous at all scales, influenced by features from overall structure to the fabric of individual lithologies that comprise them (Cocco et al., 2023; Faulkner et al., 2010).

These complexities are amplified by observational limitations: most fault processes occur at inaccessible depths and can only be studied through surface or near-surface observations, which have limited sensitivity and resolution. This hinders our ability to observe small-scale processes, such as the effects of shear-induced fault dilation (Selvadurai and Selvadurai, 2025). Although this dilation may be only a few millimetres, it can significantly influence key aspects of rupture dynamics (e.g. Brantut, 2020; Frank, 1965; Lockner and Byerlee, 1994; Proctor et al., 2020; Rice, 1975; Scuderi et al., 2015; Segall and Rice, 1995).

1.1 Open, fundamental science questions

One key question in earthquake dynamics is whether ruptures start gradually or abruptly. In models that assume ruptures to occur on smooth, infinitesimally thin planes governed by friction (e.g. Dieterich, 1978), dynamic ruptures typically result from a slow, progressive zone of accelerated slip (e.g. Dieterich, 1979; Ohnaka, 1992; Rice and Cocco, 2007; Rice, 1993). Laboratory experiments have replicated this behaviour. However, slip surfaces are more realistically non-planar, featuring topography (Candela et al., 2009, 2011; Kirkpatrick and Brodsky, 2014; Renard and Candela, 2017; Brodsky et al., 2015). In these cases, load-bearing contact points (asperities) form on principal slipping zones (Aki, 1979; Dieterich and Kilgore, 1994; Selvadurai and Glaser, 2016), and structural complexity can create strong, cohesive regions that act as rupture barriers (Aki, 1984; Ohnaka, 2003). Such complexity produces heterogeneous distributions of stresses, fluids or frictional properties that evolve with slip (e.g. Sagy et al., 2007), influencing earthquake nucleation. Studying such complexity can only be achieved in the laboratory and numerical models (e.g. Barbot et al., 2012; Cattania and Segall, 2021; Kaneko et al., 2010; Selvadurai et al., 2023; Wu and Barbot, 2025). For natural earthquakes, inferring onset phenomena is challenging, and even the observations themselves tend to be debated, since they often rely on model-dependent processing (Bletery and Nocquet, 2023; Colombelli et al., 2014; Ellsworth and Beroza, 1995; Meier et al., 2016, 2017, 2020) and are affected by instrument sensitivities (Kaneko and Ampuero, 2011; Tullis, 1996).

Fundamental questions in earthquake mechanics that remain unsolved because of a lack of direct in situ observations include *i)* the energy balance of dynamic ruptures and dissipation mechanisms controlling rupture propagation (Abercrombie and Rice, 2005; Cocco et al., 2016, 2023; Kammer et al., 2024; Selvadurai, 2019); *ii)* resulting scaling relations between small and large earthquakes, in terms of fracture energy, rupture speeds, finite dimensions, and static stress drops (Abercrombie, 2021; Abercrombie et al., 2025; Baltay et al., 2024; McGuire and Kaneko, 2018; Kurzon et al., 2020); *iii)* mechanisms of rupture arrests and corresponding seismic wave radiation (Mai et al., 2017; Mosconi et al., 2025; Ripperger et al., 2007; Kurzon et al., 2018); *iv)* the role of fluids in slow and fast fault deformation (Behr and Bürgmann, 2021; Bürgmann, 2018; Saffer and Tobin, 2011); *v)* the mutual interactions between fault zone structure, geometrical and rheological complexity, corresponding stress fields, seismicity, and larger dynamic ruptures (Ben-Zion, 2008); and *vi)* the ubiquity of precursory phenomena, such as foreshocks and changes in seismicity patterns (e.g. clustering, rate

changes, and localisation), slow deformation e.g. in the form of precursory fault slip (Bouchon et al., 2011), and other geophysical and geochemical precursors that remain widely discussed (Cicerone et al., 2009; Conti et al., 2021; Mignan et al., 2021; Scholz et al., 1973).

1.2 Insights from laboratory experiments

The study of earthquake mechanics has traditionally relied on laboratory experiments and numerical modelling (Scholz, 2018). Laboratory tests are conducted on intact rock samples, frictional bare rock surfaces, fault analogue materials (Rosenau et al., 2017), and rock powders (i.e., gouges, Marone, 1998). Sample sizes range from millimetres to metres in length and aim to investigate fault mechanics under conditions relevant to both creeping sections—where slip rates can be as low as millimetres per year—and dynamic rupture, which involves slip rates up to metres per second. Laboratories have been instrumental in developing constitutive laws governing earthquake mechanics under controlled environmental and loading conditions (Dieterich, 1979; Dieterich and Kilgore, 1994; Goldsby and Tullis, 2011; Ohnaka, 2003; Ruina, 1983). These experiments have provided unique insights into phenomena such as transitions from slow to fast sliding (Leeman et al., 2016), the conditions controlling the brittle-ductile transition (Meyer et al., 2024; Paterson and Wong, 2005), precursory slip during earthquake nucleation (Dieterich, 1978), seismicity patterns during rock failure (Goebel et al., 2012, 2014; Lockner, 1993; Lockner et al., 1991; Main et al., 1992), and thermal weakening at coseismic slip rates (e.g. Di Toro et al., 2011; Goldsby and Tullis, 2011). Monitoring conditions in such experiments, at a distance of a few millimetres or even micrometres from the fault, are much better than in a typical natural setting. Moreover, in some experiments, the rupture tip dynamics can even be monitored visually with using high-speed cameras in photo-elastic materials (Latour et al., 2013; Lu et al., 2007; Rubino et al., 2017). Nevertheless, a fundamental limitation of laboratory experiments is that it is unclear how well the mechanical response of experimental fault reproduces processes at natural, larger scales. It is uncertain to what extent millimetre- to metre-sized samples reflect the behaviour of real kilometre scale fault zones at depth (Chester et al., 1993; Faulkner et al., 2010; Shipton et al., 2006; Ben-Zion and Sammis, 2003). In this framework, it is still an open scientific question if and how the parameters controlling the constitutive equations, extracted from laboratory experiments, need to be scaled or reshaped to represent with numerical models the phenomena occurring in kilometre scale fault zones.

1.3 Induced seismicity at the field scale

Over the past decade, field-scale induced seismicity experiments have facilitated a wide range of earthquake mechanics-related observations in natural geological settings. Earlier studies focused on demonstrating the causal relationship between fluid injection and seismicity (Langenbruch and Zoback, 2016; Schultz et al., 2018; Weingarten et al., 2015). Theoretical considerations have suggested upper limits for maximum moment release, based on the amount of injected fluid (Galis et al., 2017; McGarr, 2014; van der Elst et al., 2016). Some cases exhibit apparent scaling relationships between injected volume and seismic moment release (Bentz et al., 2020; Kwiatek et al., 2019; Schultz et al., 2025). The spatial footprint of induced seismicity also seems to vary, depending on the causal mechanism (Goebel and Brodsky, 2018). Small-scale laboratory tests have also been performed to refine our physical understanding between fluid injection and induced seismicity (Goebel et al., 2024; Wang et al., 2024; Ye and Ghassemi, 2018). However, field-scale studies of induced seismicity tend to suffer from the limited sensitivity and resolution of their monitoring networks, and from imprecise knowledge of material heterogeneities or structures.

1.4 In situ experiments

There is a long tradition of studying fault behaviour using mining-induced seismic events (Gibowicz and Kijko, 1994; Langenbruch and Zoback, 2016; Schultz et al., 2018; Weingarten et al., 2015; McGarr, 1976). In the last thirty years, larger scale in situ experiments have been developed in natural settings to study or even activate natural faults under semi-controlled conditions. Especially in deep mines in South Africa, several multinational experiments combining multi-parameter high-resolution monitoring with semi-controlled loading of pre-existing fault zones were established. The See-SA project focussed on monitoring stress, strain, and slow slip deformation before, during and after slip conducted a series of experiments from 1992 to 2005 (Naoi et al., 2006; Yamada et al., 2007; Ogasawara, 2002). The NELSAM/DAFSAM Project combined seismic observations with rupture plane mapping (Heesakkers et al., 2011). The JAGUARS project in Mponeng Gold Mine successfully monitored the full life cycle of a Mw1.9 seismic event from 30 m distance at 3.5 km depth (Yabe et al., 2015). With high-sensitivity seismic monitoring, over 2 million seismic events were recorded, including fore- and aftershocks, with magnitudes -5 < Mw < 1.9 (Naoi et al., 2011; Plenkers et al., 2010). In addition, high-resolution strain monitoring and tilt monitoring as well as core analyses from the rupture plane (Yabe et al., 2015) allowed characterization of stress state, aseismic slip, and the geochemical environment (Kozłowska et al., 2015; Ziegler et al., 2015).

Further experiments that focussed on injection-induced seismicity were initiated in the Underground laboratory in Äspö (Kwiatek et al., 2018; Zang et al., 2016), at the Grimsel Test Site, the Sanford Underground Research Facility, the Underground research Laboratory Mizunami (Ishida et al., 2019), the Reiche Zeche (Blanke et al., 2023; Boese et al., 2022; Renner et al., 2021), the Mont Terri Rock Laboratory (Zappone et al., 2021; De Barros et al., 2023), the Laboratoire à Bas Bruit (Derode et al., 2015; Guglielmi et al., 2015a, 2021), and the Laboratoire de Recherche Souterrain de Tournemire (Guglielmi et al., 2015b). In particular the experiments at the Laboratoire à Bas Bruit of 2015 demon-

strated how direct on-fault observations can provide the missing link between small-scale laboratory experiments, and the larger, natural scale (Cappa et al., 2019). They measured deformation directly on an activated carbonate fault zone at a depth of 200–300 m (Guglielmi et al., 2015a), with a SIMFIP probe ('Step-rate Injection Method for Fracture In situ Properties,' Guglielmi et al., 2014), directly at the fluid injection point. This enabled a characterisation of the interplay between seismicity, aseismic deformation, and the controlled fluid pressure increase: in the beginning of the injection, fault dilation and aseismic shear slip would grow by approximately equal amounts, until the dilation reached a maximum at 0.5 mm, while the shear deformation kept accelerating for another 200 s. Microseismic activity would start only when the aseismic slip zone exceeded the pressurized zone.

These detailed observations show the potential value of direct on-fault measurements from in situ experiments. However, with the fault deformation measured only at a single point, the actual distributed fault deformation patterns, and the pore pressure evolution away from the injection point, were still under-constrained. Their inference of the fluid pressure and aseismic slip fronts, and of fault frictional properties, therefore, remain model dependent (Larochelle et al., 2021). To observationally constrain how fluid pressure, strain and stress fields evolve over time and space, across natural fault zones, requires monitoring at a higher spatial resolution and with multi-disciplinary monitoring systems.

1.5 The BedrettoLab and the FEAR project

The *Bedretto Laboratory for Geosciences and Geoenergies* (BedrettoLab, or BULGG, Giardini et al., 2022; Ma et al., 2022; Rast et al., 2022) facilitates such extensive instrumentation, because it provides direct access to natural fault zones in an in situ setting. For the ERC Synergy funded Fault Activation and Earthquake Rupture (FEAR) project, we are in the process of instrumenting a carefully selected target fault zone (Achtziger-Zupančič et al., 2024), to induce and study M_w ~1.0 dynamic earthquake ruptures. The goal is to advance our understanding of earthquake physics and hydromechanics, by monitoring earthquakes of substantial size with high sensitivity and resolution directly where they occur. In this paper, we describe the FEAR project plans and goals, the testbed buildout status, and briefly describe the suite of already conducted preparatory experiments. In Section 2 we describe the project goals, the characteristics of the target fault zone, the experiment control and the monitoring systems, and outline the already completed and planned experiments. In Section 3 we discuss the scientific insights the FEAR project can potentially deliver.

2 The FEAR project

2.1 Project goal & overview

The BedrettoLab is located in the central section of the Bedretto tunnel, a 5.2 kilometre long tunnel in the southern Swiss Alps, with an overburden of up to 1.5 km (Giardini et al., 2022; Ma et al., 2022). The tunnel initially crosscuts crystalline metamorphic units of the Helvetic domain and then penetrates into the Rotondo granite, a pre-Alpine granitic body (Ceccato et al., 2023; Rast et al., 2022), for the remaining ca. 4 km (Figure 1). The underground laboratory currently contains the 'Geoenergies Testbed' at 2,000 - 2,100 m into the tunnel, equipped with an extensive 3D multi-domain geophysical monitoring array (Plenkers et al., 2023) and a fluid injection control system, which has been used for various experiments since 2021.

Some 400 metres further into the Bedretto tunnel, we are now building the interdisciplinary 'Earthquake Physics Testbed' around the target fault zone of the FEAR project: a steeply dipping, ~2 m wide granitic fault zone, which has been selected with a multi-disciplinary characterisation and selection procedure (Achtziger-Zupančič et al., 2024) (Section 2.2). We are in the process of building a remotely run experiment control system and an extensive monitoring system (Section 2.3) directly onto and around this natural fault zone. This includes the 110 m long FEAR tunnel that runs parallel to the fault zone at a lateral distance of 40 m. From both the FEAR and Bedretto tunnels, we drill monitoring, injection, and production boreholes through or towards the fault zone, to place sensor and experiment control equipment. In a sequence of fault activation experiments (Section 2.4), we aim to monitor the major relevant observables for coupled thermo-hydro-mechanical earthquake processes, notably strain, ground motion, fluid pressures, and temperature, along with other, somewhat less conventional observables, such as hydrogeochemical and microbiological features of fault-associated fluids.

With fluid injections at multiple injection points, we will then attempt to re-activate the fault zone and to induce 10-100 m long dynamic earthquake ruptures (M_w~1.0). The multi-disciplinary and multi-scale monitoring system should allow us to characterise complex rupture processes from close distance.

As such, FEAR builds on the pioneering past fault activation experiments, and attempts to scale them up significantly in terms of *i)* greater depth: at 1.0-1.5 km beneath the surface, we are reaching the seismogenic depth range with stress and faulting conditions relevant for natural earthquakes and with frictional properties expected to change from stable to unstable; *ii)* the scale of the target events: we attempt to trigger events with M_w ~1.0 and rupture lengths of 10-100 m, within our monitoring arrays; *iii)* the extent to which the fault zone and the surrounding host rock can be characterised, because of the direct fault zone access the BedrettoLab provides; *iv)* the level of experiment control: with packer systems that enable targeted injections into narrow fault zone segments, and with simultaneous fluid injections via multiple injection boreholes; *v)* the extensive multi-scale and multi-disciplinary instrumentation, combining on-fault strain, borehole tilt, pressure, and temperature measurements with an extensive multi-scale seismic network; and *vi)* the integration of in situ experiments, field geology, numerical modelling,

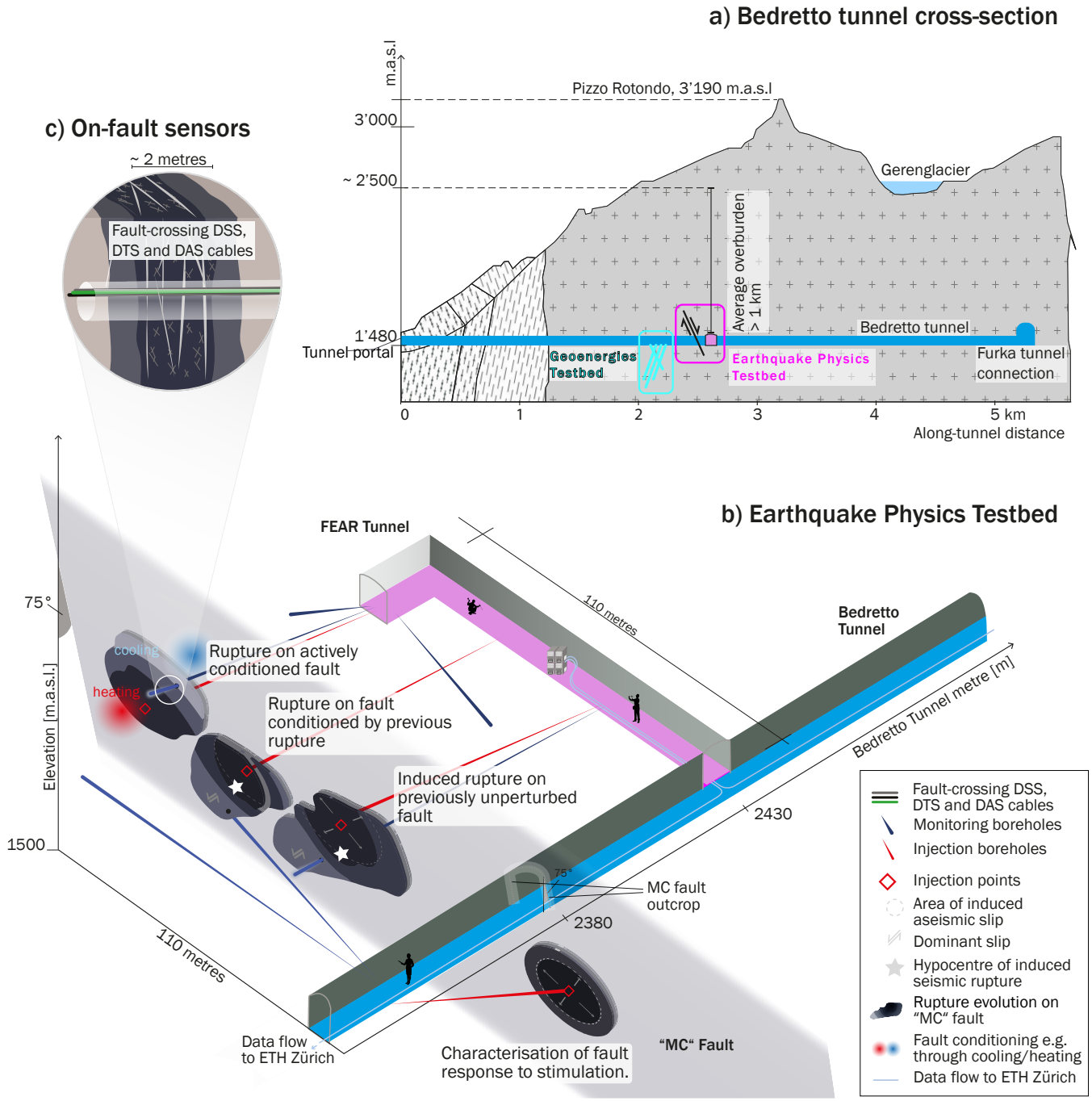

Figure 1 The Earthquake Physics Testbed at the BedrettoLab is being built for the FEAR project, approximately 2.4 km along the Bedretto tunnel (blue floor). The recently completed fault-parallel FEAR tunnel (pink floor) provides access to the steeply dipping target fault zone ('MC fault'), and to the planned fault segments that will be targeted in a suite of fault activation experiments (Section 2.4). The first experiment to the south-west of the Bedretto tunnel (bottom right segment) has already been conducted in November and December of 2024. The remaining experiments are planned for2026 and 2027.

and accompanying rock mechanics laboratory experiments.

The in situ experiments are accompanied by rock deformation laboratory experiments on five different, complementary machines at three experimental rock-deformation laboratories, at the RPMLab of ETH Zurich (LabQUAKE, Salazar Vásquez et al., 2024), the HPHT Lab at INGV Rome (SHIVA, Aretusini et al., 2024; Cornelio et al., 2024; Di Toro et al., 2010; BRAVA, Collettini et al., 2014; Pozzi et al., 2023; Volpe et al., 2023; MEERA, Spagnuolo et al., 2023), and at the GUT Lab of RWTH Aachen (Osten et al., 2024). By combining extensive in situ observations with laboratory experiments, numerical process models and geological studies, we aim to understand microphysical processes that drive earthquake rupture dynamics.

2.2 Target fault zone

The selection and characterisation procedure of the FEAR target fault zone (Achtziger-Zupančič et al., 2024)

has combined geological characterisation at the field and tunnel scale, borehole logging and core analyses, geophysical investigations with ground-penetrating radar (GPR, Figure 2), hydrogeological and stress characterisation, mineralogical and petrographic analyses, and rock deformation tests. The target structure, termed 'MC fault', was chosen because of: *i)* its relatively simple geometry and sufficient spatial extent to host multiple M~1.0 ruptures; *ii)* its relatively favourable orientation with respect to the in situ local stress field; *iii)* the presence of gouge material on some of the fault zone strands, indicative of localised slip in the past; and *iv)* its limited fluid transmissivity, as evidenced by relatively low fluid outflow compared to other candidate structures.

The selected target fault is a tectonically immature structure characterised by numerous discrete brittle shear planes, confined in a volume of roughly 2 metres width, in sharp contact with the relatively intact host rock, the Rotondo granite (Figure 3). The main shear strand (labelled '#48.1' in Figure 3) is sub-parallel to other, more minor strands, and dips 58° northwest, striking almost perpendicular to the Bedretto tunnel. The dip of the macroscopic fault zone is somewhat steeper (~75°) than the main individual fault zone strands. GPR measurements from the nascent FEAR tunnel confirm the spatial extent and simple geometry of the target fault zone for at least 80 m to the southwest of the Bedretto tunnel (Figure 2). Remote sensing investigations of deformation structures observed at the ground surface suggest that such structures tend to span >100 metres in length, being composed of single fracture planes with an average length of 30-50 m (Achtziger-Zupančič et al., 2024).

The fault is classified as immature, as it is characterized by a simple slip surface defined by a centimetre-thick fault core and lacking a well-developed damage zone at the metre scale. This suggests high degrees of strain localisation within the main fault strand #48.1. This strand presents far larger fluid outflow than the fracture network, and thus it may be acting as a channelised conduit (Caine et al., 1996). The fault core and slip plane are lined by an up to 5 cm thick, discontinuous layer of gouge and cataclasite (Figure 4), which represent the natural fine-grained product of brittle shearing through cataclasis of the fractured host rock (Volpe et al., 2023). The geological evolution of the fault includes an initial activation under high-temperature, ductile deformation conditions with a thrust–reverse shear sense (Ceccato et al., 2024), followed by strike-slip reactivation at shallow crustal levels, as indicated by sub-horizontal slickenlines and grooves on the fault plane. Although direct field constraints on the total displacement are lacking, the fault core thickness of ~0.01–0.1 m suggests a cumulative displacement on the order of ~1 m during the shallow faulting activity, based on scaling laws for similar faults in granitic rocks (Shipton et al., 2006; Torabi and Berg, 2011). The spatial distribution and prevalence of gouge layers and bare-rock contacts across the fault zone are not yet known, and it is currently unclear if the gouge layers dictate the frictional stability of the fault zone, or if they are merely a passive result of localised fault deformation.

In the estimated background stress field from near the Geoenergies Testbed, the fault has an intermediate slip tendency (shear stress divided by normal stress) of ~0.3, and is expected to slip in an oblique, right-lateral dip-slip sense (Bröker et al., 2024b; Bröker and Ma, 2022; Hamdi et al., 2025). More updated stress field characterisations using observations from the Earthquake Physics Testbed boreholes are under way. At 7 MPa, the in situ pore pressures on and around the target fault zone are below hydrostatic conditions (given the ~1 km overburden). This is common in the Bedretto-Lab (Bröker and Ma, 2022), presumably because of the water drainage via the main tunnel since its creation in 1973. A small drainage conduit runs along the floor of the tunnel, collecting water inflow from the rock mass and fractures that transect the tunnel. It continuously drains between 1,000 - 6,000 l/min, preventing the tunnel from flooding, and providing water for injection experiments. Water physicochemical parameters monitored at the drainage exhibit a temperature range of 16.5-17.5 °C, a pH of 8.3-8.7, and an Electrical Conductivity (EC) of 80-95 µS/cm. In contrast, borehole groundwater sampled along the MC fault demonstrated a slightly higher temperature range of 18.5-22.5 °C, a pH range of 8.4-9.0, and an EC range of 80-160 µS/cm. These differences facilitate the detection of water inflow into boreholes with DTS monitoring (Section 2.3), and into the tunnel.

Laboratory experiment characterisation of fault gouge material from where strand 48.1 intersects the Bedretto tunnel (Volpe et al., 2023) suggest that the natural fault gouge material is characterised by: *i)* an intermediate friction coefficient (μ = 0.49), i.e. lower than Byerlee's friction of 0.85; *ii)* low cohesion (c < 0.2 MPa); *iii)* velocity strengthening friction (rate-and-state a-b parameter of 0.0025); *iv)* moderate to high healing rates ($\beta = \Delta\mu/\log10(t)$ ~0.005); and *v)* moderate shear-perpendicular permeability (10^{-17} and 10^{-16} m^2), higher than in the host rock (10^{-19} m^2, Osten et al., 2024). Despite the velocity strengthening friction, laboratory fluid injection tests performed at in situ conditions show that unstable reactivation with fast slip on the experimental fault can be reached (Volpe et al., 2023) because of competing effects of dilatancy, stabilizing shear failure in rock (Aben and Brantut, 2021), and pressure build up by fluid injection and shear compaction (e.g., Zhong et al., 2025).

Fault zone characterisation, and the compilation of a detailed, observation-driven fault zone model, is a core aspect of the FEAR project. The model is continuously being improved, and it is informed by ongoing characterization campaigns on various aspects of the fault zone and host rocks, including fault zone structure, the local stress field, hydraulic and hydro-mechanic properties, as well as fault surface roughness, mechanical strength, and frictional characteristics.

2.3 The Earthquake Physics Testbed

Around this target fault zone, we are building the Earthquake Physics Testbed, a research infrastructure that

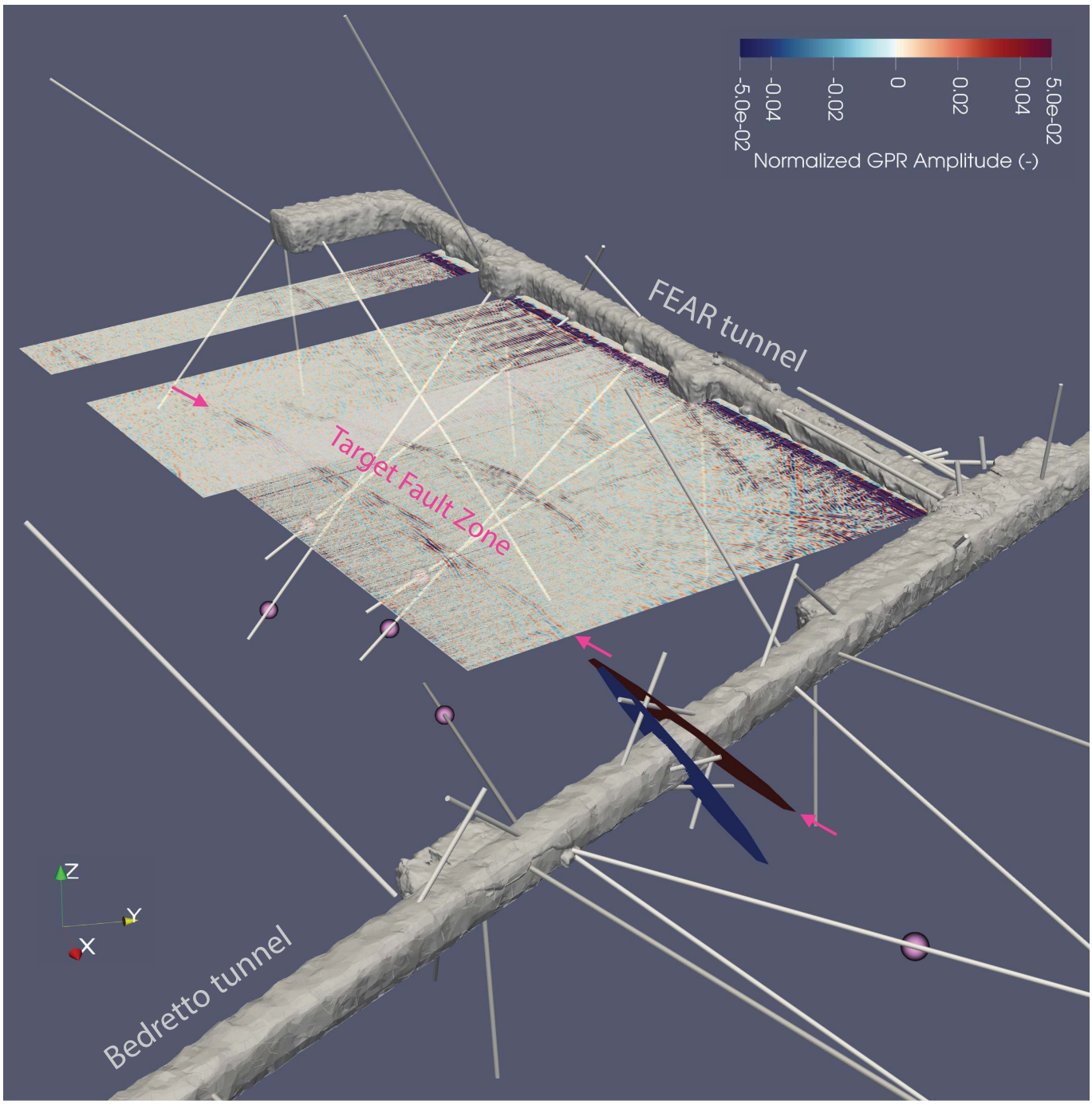

Figure 2 Tunnels, boreholes, and GPR image of the FEAR target volume, acquired from the newly excavated FEAR tunnel. The FEAR target fault zone (pointed at by pink arrows) is discernible as a relatively isolated, well defined structure, with some geometrical complexity at 40m distance, parallel to the FEAR tunnel. The major strands of the target fault zone are highlighted as a red and blue disk where they intersect the Bedretto tunnel. Places where boreholes cross the fault zone are marked with a pink sphere. Geographic north is in the positive y-direction.

aims to facilitate fault activation and other fluid injection experiments, with exceptional experiment control and process resolution. The monitoring system is designed to facilitate the mapping of all observables that are relevant for earthquake faulting processes, before, during and after the main ruptures, across the experimental volume, and across a wide range of scales (Figure 5).

The Earthquake Physics Testbed is facilitated by the fault-parallel FEAR tunnel (Figures 1, 2 & 5). It allows placing sensors and injection packers on and near the fault with relatively short (ca. 50 m) boreholes. Tunnel construction was completed in June 2025 and is now followed by a buildout and instrumentation campaign that includes a total of 40 monitoring and injection boreholes. The boreholes are designed to provide a large array aperture vertically (±40 m) and laterally (ca. 200 m), good spatial coverage of the entire experiment volume, and high process sensitivity and resolution, especially near the fault. Different boreholes can host a wide range of sensors (Table 1, Figure 6), as described in more detail below. Additionally, monitoring equip-

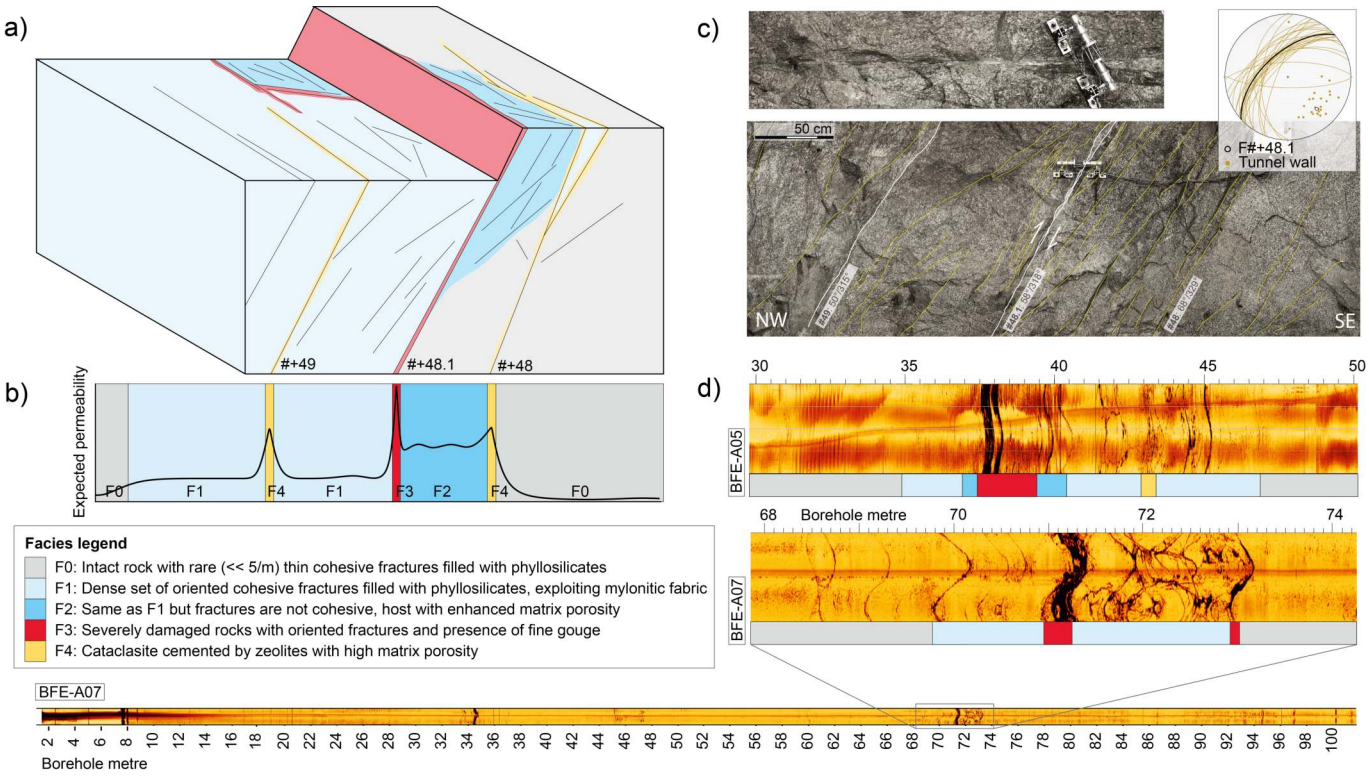

Figure 3 Target fault zone of the FEAR project. **(a)** Conceptual fault zone model with 5 distinct facies, and **(b)** expected, qualitative fluid permeability. **(c)** Photograph of the intersection of the target fault zone with the Bedretto tunnel (bottom); rotated close-up view of the main strand (#48.1, top) which hosts the gouge material studied in Volpe et al. (2023) and across which a DORSA strain probe is installed; and stereonet (top right) of the main strand (black line) and secondary structures (yellow lines), shown as great circles and their poles. The shear indications on strand #48.1 reflect the deformation sense during the early stages of fault zone evolution (see text), rather than the expected shear sense in the current stress field. **(d)** Acoustic televiewer logging image of the target fault zone in two fault-crossing boreholes (BFE_A05 and BFE_A07) across the first 100 m of the borehole (bottom), and close-up views where the borehole intersects the target fault zone.

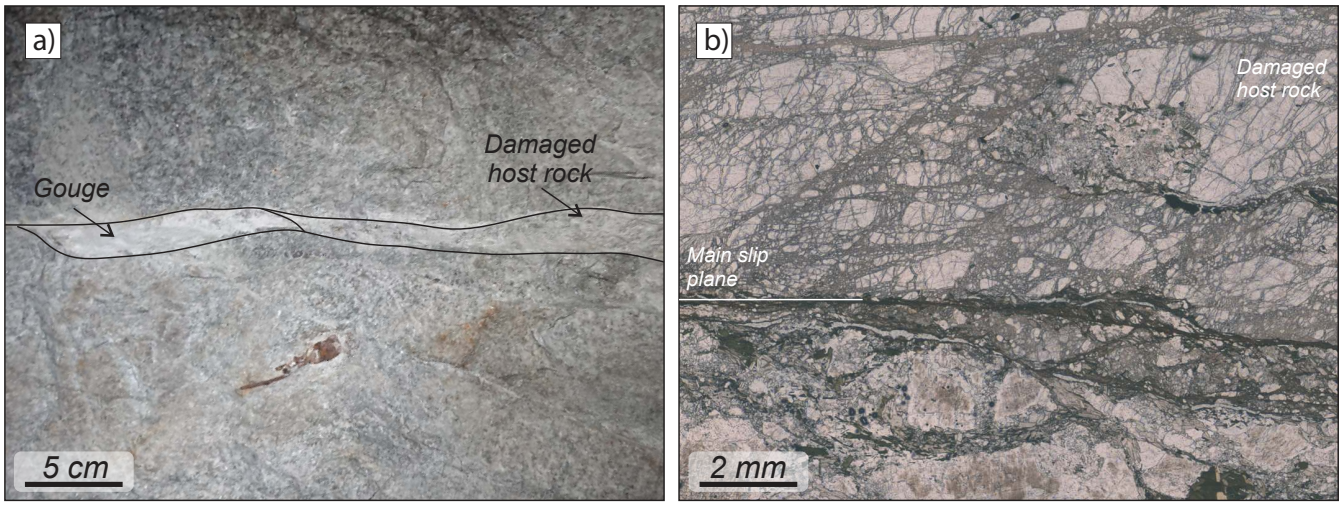

Figure 4 **(a)** Close-up view of the target fault plane on the NE tunnel wall (strand #48.1, sampling site of the gouge analysed in Volpe et al., 2023). **(b)** Detail of the microstructures of the man slip plane of the target fault zone showing the thin layer of gouge developed along the main slip plane, and the damaged host rock that is observed only in a few places along the fault.

ment is also placed along the walls and floors of the two tunnels, as well as at the topographic surface. The target fault zone to the north-east of the Bedretto tunnel was already instrumented in June–November 2024, before the FEAR tunnel was completed, and has hosted the FEAR-1 experiment (Section 2.4).

2.3.1 Experiment control

Fluid injections into the target fault zone can be made via up to four stimulation boreholes in the south-west segment of the Earthquake Physics Testbed, and two in the north-east segment. To overcome the in-site pres-

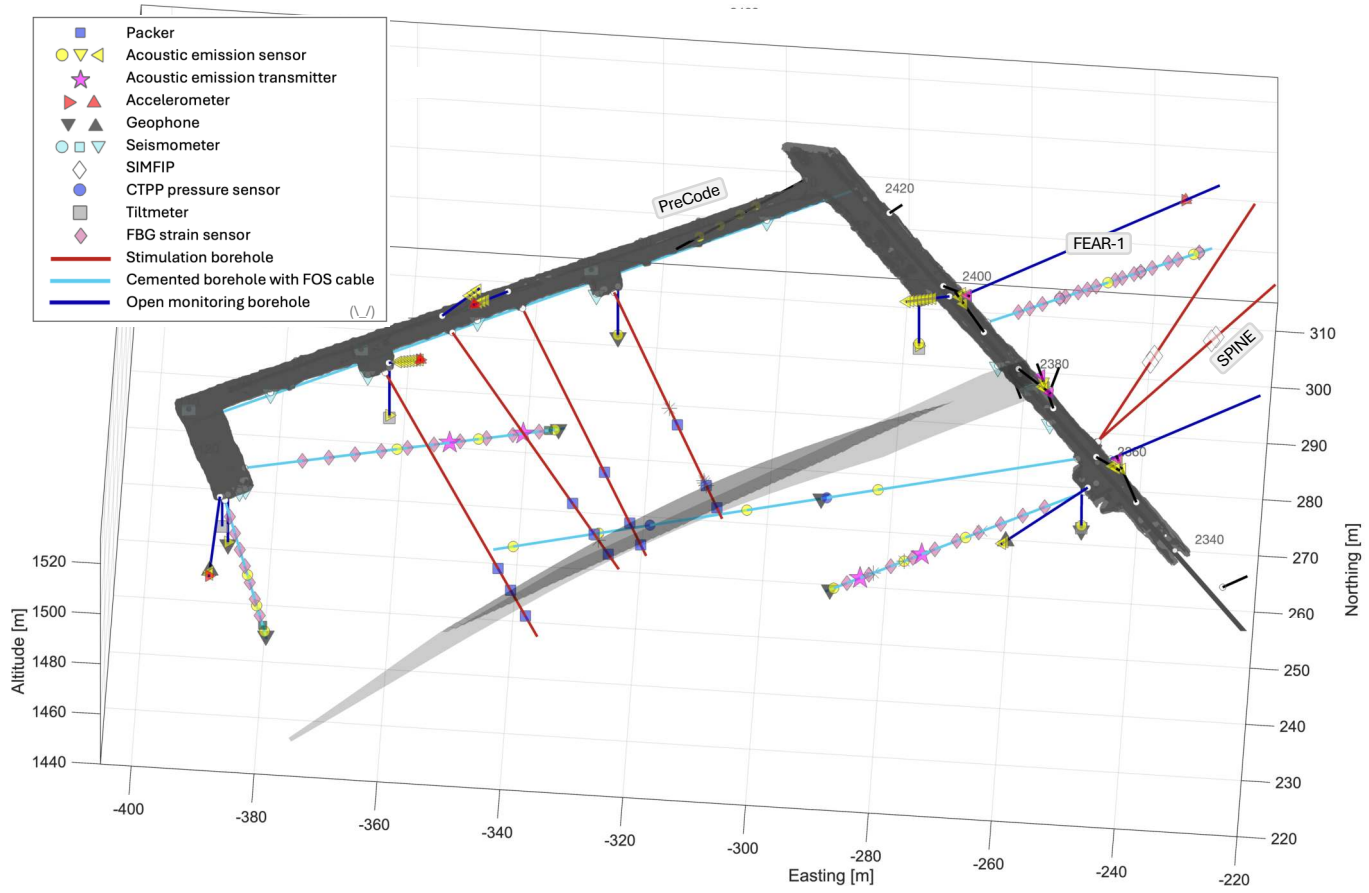

Figure 5 Earthquake Physics testbed setup and monitoring system, with completed boreholes and planned sensor installations, around the MC target fault (grey surface). The labelled experiments are described in Section 2.4. An animated 3D version of this figure is provided as electronic supplement.

sure and stresses acting on the fault zone, injection pressures of some 20-30 MPa are required. To achieve such pressure, high flow rates may be necessary, depending on the local hydraulic properties at the individual injection points. For this purpose, we have designed a modular flowline and injection scheme, where we can run arbitrary combinations of pumps in parallel and in series to the different injection boreholes. A total of six pumps (Speck triplex pump P45_320 with Hitachi SJ-P1 controller) with up to 45 l/min at 32 MPa are available. Each group of pumps can be individually controlled, which facilitates simultaneous injection at all boreholes, and complex injection strategies with alternating or asymmetric injections, with individual injection protocols per borehole.

For safety reasons, attendance in the tunnel is not allowed during high-rate injections. All experiment control and monitoring systems are remote-controlled from the command centre on the ETH Zurich main campus in Zurich. The system includes fail-safe procedures to shut down pumps and vent the injection boreholes for scenarios of unexpected behaviour (see Section 2.5), communication problems, discontinued water supply, etc. Moreover, injection protocols can be preprogrammed, and longer-term injections can be run largely autonomously and in a highly repeatable fashion.

2.3.2 Data flow

Data from the experiment control and monitoring system is live-streamed (10 Gbps network capacity), processed, and archived in real-time at a dedicated BedrettoLab computational facility hosted in server rooms of ETH Zurich. The facility consists of several massive-multicore shared memory machines on which virtual server entities can be flexibly assigned to analysis tasks as needed.

2.3.3 Pressure and strain monitoring

For controlled fluid injections to stimulate faults or fractures into narrow target intervals, we use high-pressure steel-reinforced rubber straddle packer systems, and, in some cases, SIMFIP probes (Guglielmi et al., 2014). The latter combine measurements of fluid pressure within the injection intervals, with a co-located fibre optic sensing array to measure 3D displacement (Figure 6). Borehole axial and radial displacement range are ±0.7mm and ±3.5mm and resolution is 0.1µm. A compass allows orientation of the three-dimensional measurements in magnetic or geographic coordinates. The displacement sensor also measures the rotations around the three orthogonal axes with a range of 0.04 radians and a resolution of 0.1 µradians.

In specific fault-crossing monitoring boreholes that are not used for injection, as well as on the target fault

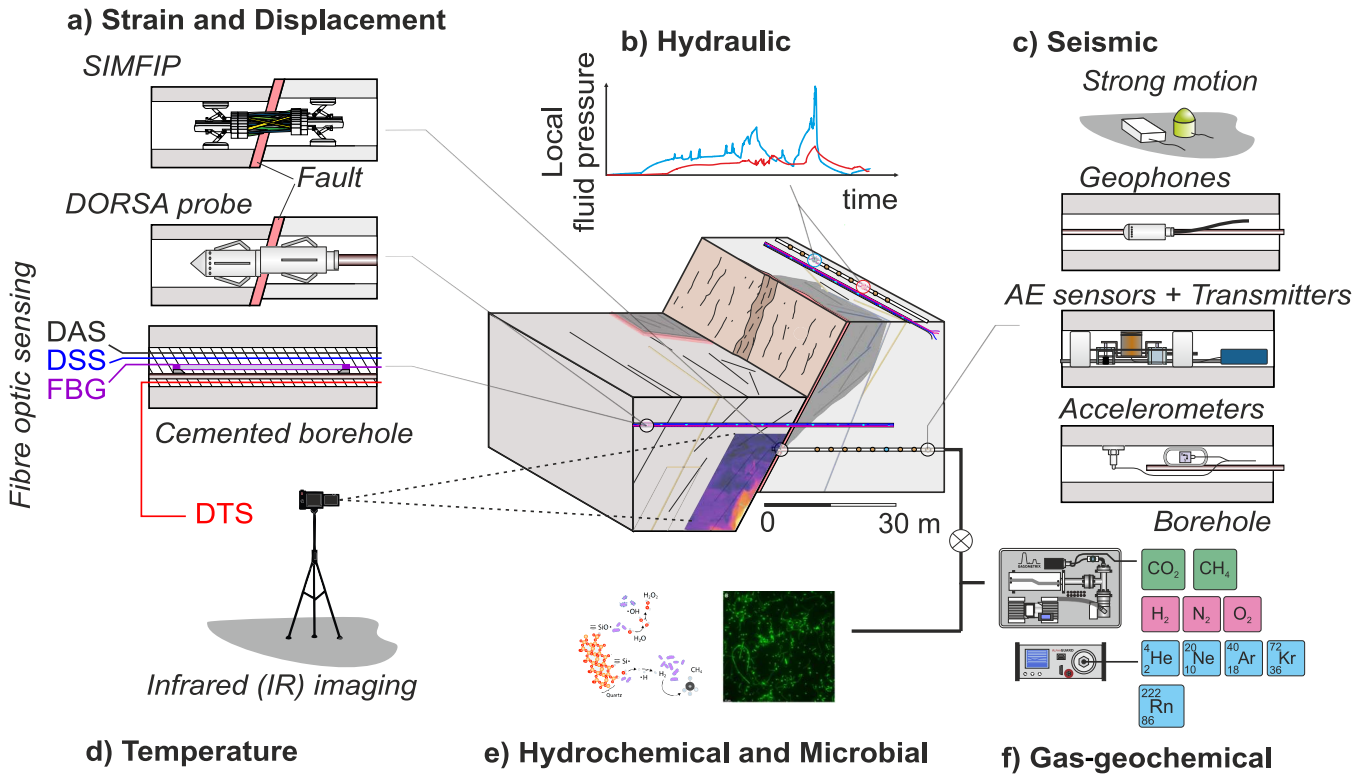

Figure 6 Selected elements of the FEAR integrated monitoring system described in the text.

outcrop of the Bedretto tunnel wall (Figure 3c), we place DORSA probes ('Downhole Robotic Strain Analyzer'). DORSAs are advanced, passive versions of the SIMFIP injection probes, with the same 0.1 µm resolution but an increased displacement range (±2.5 mm axial and ±25.0 mm radial). Furthermore, DORSAs monitor rotations with a 0.17 radians range and 0.1 µradians resolution. These on-fault probes can reveal the temporal evolution of fault shearing, dilation, and compaction at or near the injection point.

In addition to the pressure monitoring via the straddle packer systems, tube pore pressure sensors (CTPP, Plenkers et al., 2023) are installed in cemented monitoring boreholes. These sensors are co-located with Fibre Bragg Grating sensors with the goal of complementing the understanding of the poroelastic responses (Dutler et al., 2021). The CTPP sensors measure fluid pressure in a hydraulic setting that is expected to evolve both during individual experiments and between subsequent injections (Krietsch et al., 2020). At locations where these sensors are surrounded by hydraulically tight rock, their response can be seen as nearly undrained because the pore water volume remains nearly constant. At locations where they are installed across a fracture, a drained response is possible, because of the enhanced hydraulic conductivity. In addition, we install borehole tilt meters in sub-vertical boreholes that lie in the vicinity of the fault (Figure 5). We use the self-levelling Lily 500 series, which can achieve a resolution of up to 5 nanoradians.

2.3.4 Distributed fibre optic sensing

Furthermore, fault-crossing and fault-parallel cemented boreholes are equipped with tight buffered and loose tube fibre-optic sensing (FOS) cables with both single-mode and multi-mode fibres, allowing for simultaneous Distributed Acoustic (DAS), Strain (DSS) and Temperature (DTS) sensing. For DAS we will be using newly developed interrogators that can provide data with a small (4 m or below) gauge length up to 10 kHz sampling (depending on final interrogation length), with spatial sampling as low as tens of centimetres and with a sensitivity of ~10 nano-strain rate. For DSS, we will be using both Rayleigh- and Brillouin-based interrogation units that provide relative and absolute strain with smallest spatial resolution of 5 and 50 cm, respectively. The accuracy, measured in the field, is 0.1 micro-strain for the Rayleigh relative measurement and 5-10 micro-strain for Brillouin absolute values. Depending on the final layout and optimization, measurements for DSS are usually taken every minute. For DTS, we rely on both Raman- and Brillouin-based interrogators, with spatial sampling of 25/50 cm and accuracy of 0.01/0.1°C, respectively. Depending on the final setup, a single measurements can be done within few seconds to several minutes. The distributed sensing systems are designed to allow determination of the spatial distribution and evolution of strain and temperature across the multi-strand fault zone. This may allow us to determine, for example, if pre-seismic deformation is distributed across multiple strands, or dominated by a single one. It also allows us to directly measure co-seismic heat anomalies, if a rupture propagates through a fault-crossing cable, up to the

Sensor type	Number installed	Number planned	Sampling rate (sps)	Placement	Data acquisition
Triple-packer with flow & pressure control	0	3	1	Borehole	5stack / MQTT
Double-packer with flow & pressure control	0	1	1	Borehole	5stack / MQTT
CTPP borehole pressure probes	3	5	1	Borehole	5stack / MQTT
SIMFIP	2	2	1k	Borehole	HYPERION si255
DORSA	2	2	1k	Borehole and tunnel wall	NiDAQ
FBG	20	44	1k	Borehole	HYPERION si255
DAS	1 borehole	5 boreholes	4k	Borehole and tunnel floor	Febus A1/Sintela Onyx
DSS	1 borehole	5 boreholes	0.016	Borehole and tunnel floor	fibrisTerre fTB5020
DTS	1 borehole	5 boreholes	0.0016	Borehole and tunnel floor	Silixa XT-DTS
Tiltmetres	3	8	1	Borehole	Raspberry Pi
Broadband seismometers	11	26	500 - 10k	Tunnel floor, posthole and surface	Nanometrics Centaur
Short period seismometers	3	3	500 - 10k	Tunnel floor, posthole and surface	Nanometrics Centaur
Broadband accelerometer	8	13	500 - 10k	Tunnel floor, posthole and surface	Nanometrics Centaur
Geophones	2	11	2k - 10k	Borehole	Nanometrics Centaur
Piezo-accelerometers	2	7	200k	Borehole	GMuG
Acoustic emission sensors	25	72	200k	Borehole	GMuG
Acoustic emission transmitters	0	4	-	Borehole	-
Seismic sparker	0	1	-	Borehole	-
Infrared camera	1	1	-	Tunnel	-
Radon - Rad8	0	2	minutes	Tunnel	-
MiniRuedi	0	1	10 minutes	Tunnel	SRS RGA200
pH meter	0	1	discrete measurement	Portable	CHAUVIN ARNOUX CA10101
Electric conductivity meter	0	1	discrete measurement	Portable	CHAUVIN ARNOUX CA10141

Table 1 Overview of sensor types installed at the Earthquake Physics Testbed, with already installed (as of 9 December 2025) and planned (March 2026) sensor counts. See text for details.

point where the cable might break. Furthermore, the DAS monitoring complements and extends the seismic monitoring with the very high-frequency AE sensors (Figure 7b).

A second fibre optic sensing cable employs linear arrays of Fibre Bragg Grating (FBG) sensors. This sensing solution can measure strain with 1 micro-strain accuracy and temperature with up to 0.1 °C resolution at 1 kHz sampling frequency. Down-sampling the data to 1 Hz further enhances strain sensitivity to 0.1 micro-strain.

2.3.5 Passive seismic monitoring

The 3D seismic monitoring system is designed to cover an extremely broad range of frequencies and amplitudes, and serves multiple purposes, including *i)* the detailed characterisation of mainshock events, *ii)* the characterisation of femto- to micro-seismicity (Table 2), *iii)* the systematic monitoring of seismicity in the wider Bedretto region, and *iv)* informing the traffic light system that we operate during experiments (Section 2.5). To achieve this, we combine various types of seismometers, accelerometers, geophones, and acoustic emission sensors and transmitters (Figures 5 & 8, Table 2). Specifically, the system combines *i)* low frequency (0 - 200 Hz) monitoring with standard high sensitivity and strong motion seismometers, to complement the BedrettoLab permanent monitoring system (Mesimeri et al., 2024); *ii)* mid frequency (100 Hz – 25 kHz) monitoring with borehole geophones and accelerometers, that can be placed close to the fault, and which can record larger amplitude signals on scale; and *iii)* high frequency (1

kHz - 100 kHz) acoustic emission monitoring, which can detect and characterise femto- to nano-seismicity.

During experiments performed in the Geoenergies Testbed (Section 2.4), we established that with such a monitoring setup we can reliably detect seismicity down to at least Mw -4 across the experimental volume (Obermann et al., 2024), and with relative hypocentre location accuracies on the order of decimetres (Rosskopf et al., 2025). The resulting seismicity patterns reveal intricate seismogenic structures (Figure 7a), which resemble the fault zone structures transecting the Bedretto tunnel, and those observed in surface outcrops (Ceccato et al., 2024). For Mw -4.0 events, the very high frequency seismic signals recorded by the AE sensors remain above the noise level in the frequency range of 1k - 10k Hz out to 20 - 40 m (Figure 7c), and to well over 100 m for Mw -2.5 events.

We operate three overlapping but separate seismic monitoring systems, which serve different purposes, and which are described in more detail below:

1. The experimental seismic monitoring system for monitoring of the experimental target volumes during stimulation experiments, based on instrumentation that may change between experiments.
2. The permanent seismic monitoring system based on the BedrettoLab permanent network, to continuously monitor and characterise seismicity in the larger Bedretto area (Figure 8).
3. The continuous standard 24/7 seismic monitoring system of the Swiss Seismological Service (SED) based on the Swiss national network.

The three systems differ in which instruments they draw data from, how closely they are monitored by human analysts, and in the parameters used for their processing. All systems are built on mutually compatible SeisComp workflows to ensure consistency and continuity between experimental and long-term monitoring datasets.

The experimental monitoring system is operated during seismogenic fluid-injection experiments. It includes temporary experiment-specific sensors, such as GMuG acoustic emission sensors configured for 200,000 samples per second data acquisition. Compared to the Geoenergies Testbed instrumentation, where seismic sensors are mostly in cemented boreholes (Plenkers et al., 2023), the Earthquake Physics Testbed instrumentation includes a larger number of upgoing boreholes, with retrievable sensors (Figure 5). In both testbeds, the data is processed automatically without manual review, enabling rapid detection and characterization of induced femto- to microseismicity. We use standard phase picking, phase association and hypocentre location workflows to compute automated seismicity catalogues. Following experiments, the catalogues undergo dedicated post-processing, including picker and locator tuning, to refine event detections and improve location accuracy.

The permanent seismic monitoring system uses all surface and tunnel stations with up to 2,000 Hz sampling rate for continuous automatic monitoring, and manual earthquake location. During high-pressure or flow-rate injections, this system is monitored by a human analyst around the clock; when no injections are being conducted, events are revised manually after they occur. The system also uses data from selected borehole instruments from the experimental system to improve the 3D network coverage. Furthermore, all instruments from the experimental monitoring system can be imported manually, to improve manual earthquake locations.

For the continuous standard seismic monitoring, the SED has continuously densified the broadband seismic network in and around the BedrettoLab, and developed the BULGG seismic network (Figure 8a, network code '8R', Mesimeri et al., 2024; Swiss Seismological Service (SED) at ETH Zurich, 2018). As of September 2025, the network consists of 7 surface stations within 10 km of the BedrettoLab, and 12 stations installed on the Bedretto tunnel floor. All the 8R surface stations are also used by the SED for 24/7 national monitoring. As a result of this regional densification, the magnitude of completeness of the SED national seismicity catalogue in the Bedretto region has been reduced from approximately 1.4 (Diehl et al., 2021) to 1.1 (Diehl et al., 2025). Earthquakes with M_{Lhc}~0.5 can often be detected as far as 8 km from the main tunnel. This network densification enables the more systematic detection of small events and better characterization of seismic sequences from the underground laboratory to regional scales. The resulting seismicity catalogue is integrated into the Swiss national database and disseminated as an open public service.

2.3.6 Active seismics

For active seismics, we conducted a comprehensive cross-hole survey around the MC fault, with 1 m spacing of both sources and receivers to ensure sufficient ray coverage for a meaningful velocity model. This dataset also provides the potential to analyse additional wavefield properties, such as attenuation, reflections from the fault zone, and possible seismic anisotropy. In addition, we integrate 3D arrays of AE transmitters with dominant frequencies in the range of 30-40 kHz (Schwarz et al., 2025). Their seismic signals remain above the ambient noise levels of the BedrettoLab across several tens of metres (Plenkers et al., 2023), supplementing the active seismic surveys and enabling inference of seismic velocity changes (Boese et al., 2022; Schwarz et al., 2025). This may allow us to map out seismic transmissivity changes across the target fault structure (e.g. from fault healing after a mainshock), and to distinguish changes on discrete interfaces from poroelastic and other volumetric effects.

2.3.7 Infrared optical monitoring

Infrared (IR) imaging of the outcrop where the fault intersects the Bedretto tunnel (Figures 2 & 3c) facilitates the measurement of temperature variations in the fault zone, especially following significant seismic events. This approach allows us to observe thermal anomalies that may arise due to frictional heating, changes in

Magnitude range	Name	Approx. source dimensions	Approx corner frequencies	Sensor types
2 to 4	Small	0.1 - 1 km	1 - 10 Hz	BBS, SPS, BBA, DAS
0 to 2	Micro	10 – 100 m	10 - 100 Hz	BBS, SPS, BBA, GPH, PAS, DAS
-2 to 0	Nano	1 – 10 m	0.1 - 1 kHz	GPH, PAS, AES, DAS
-4 to -2	Pico	0.1 - 1 m	1 - 10 kHz	GPH, PAS, AES
-6 to -4	Femto	1 – 10 cm	10 – 100 kHz	AES

Table 2 Earthquake naming nomenclature after Ellsworth et al. (2007) and Bohnhoff et al. (2009), including most important monitoring sensor types: broadband seismometers (BBS), short period seismometers (SPS), broadband accelerometers (BBA), geophones (GPH), piezo-accelerometers (PAS), acoustic emission sensors (AES), and distributed acoustic sensing (DAS). Approximate source lengths and corner frequencies are computed with the model of Brune (1970) with 3 MPa stress drop and 3.4 km/s rupture speed, and rounded for simplicity.

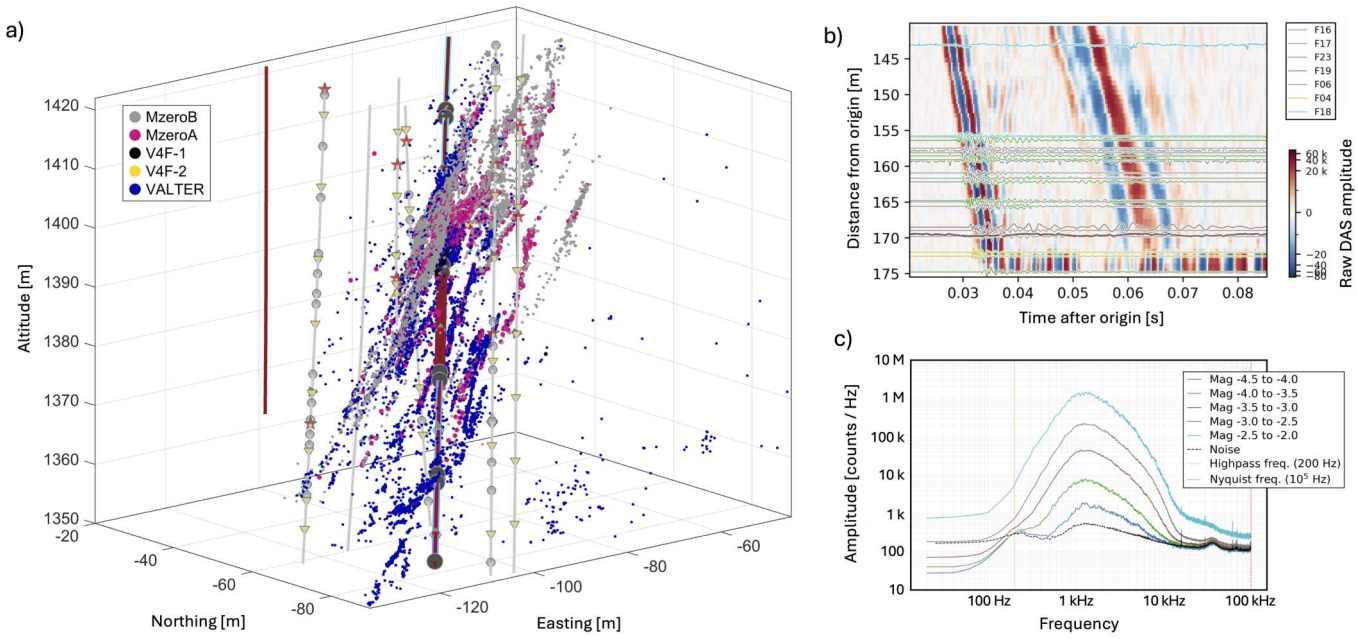

Figure 7 Geoenergies Testbed seismicity. (a) Spatial distribution of well-constrained events induced in the experiments at the Geoenergies Testbed described in the text. (b) Example records of a M_w -0.7 event recorded both on AE sensors and on a cemented DAS cable. (c) Median amplitude spectra for acoustic emission recordings in 5 separate magnitude bins, recorded at 20-40 m distance, and for ambient noise.

stress, or fluid flow triggered by seismic activity. Similarly, temperature sensors in the drainage conduit along the tunnel measure inflow into the tunnel from the fracture system.

2.3.8 Hydro-bio-chemical monitoring

In order to study the hydro-bio-chemical dynamics of the activated fault zone, we continuously monitor a wide range of hydro-chemical and microbial parameters in the water outflow at all stages of the stimulations. This includes fluid pressure and water temperature, electrical conductivity, oxidation-reduction potential, and pH, as well as discrete measurements of major anions and cations, stable water isotopes, dissolved inorganic carbon (e.g. ^{14}C-DIC), dissolved organic carbon (e.g. ^{14}C-DOC) and biological data (cell counts, DNA, and protein analyses). Furthermore, gas-geochemistry monitoring is performed with an online portable mass spectrometer ('MiniRuedi', Brennwald et al., 2016). This device monitors key gas species such as helium (He), argon (Ar), krypton (Kr), carbon dioxide (CO_2), oxygen (O_2), and nitrogen (N_2). A portable radon detector uses a Rad8 sensor to measure radon (Rn). With this comprehensive outflow monitoring, we can study fluid-gas interactions, and gas species release from the rock volume (e.g. He, Rn) during stimulation. Furthermore, the biochemical observations may reveal microbial community shifts—changes in abundance, diversity, composition, and functional potential—during stimulations. By coupling these data with subsequent microbial DNA and protein high-throughput sequencing, quantitative PCR of functional genes, and isotopic analysis (e.g. stable isotope ratios of groundwater sulphate ^{34}S/^{32}S), we can evaluate microbial metabolic activity and community structure, and how they are linked to fault zone deformation processes.

Together, all these elements form an extensive, integrated monitoring system that should facilitate accurate process characterisations from subtle potential precursory signals, to M_w~1.0 'main shock' events, and from slow fault dilation and shear transients to rapid

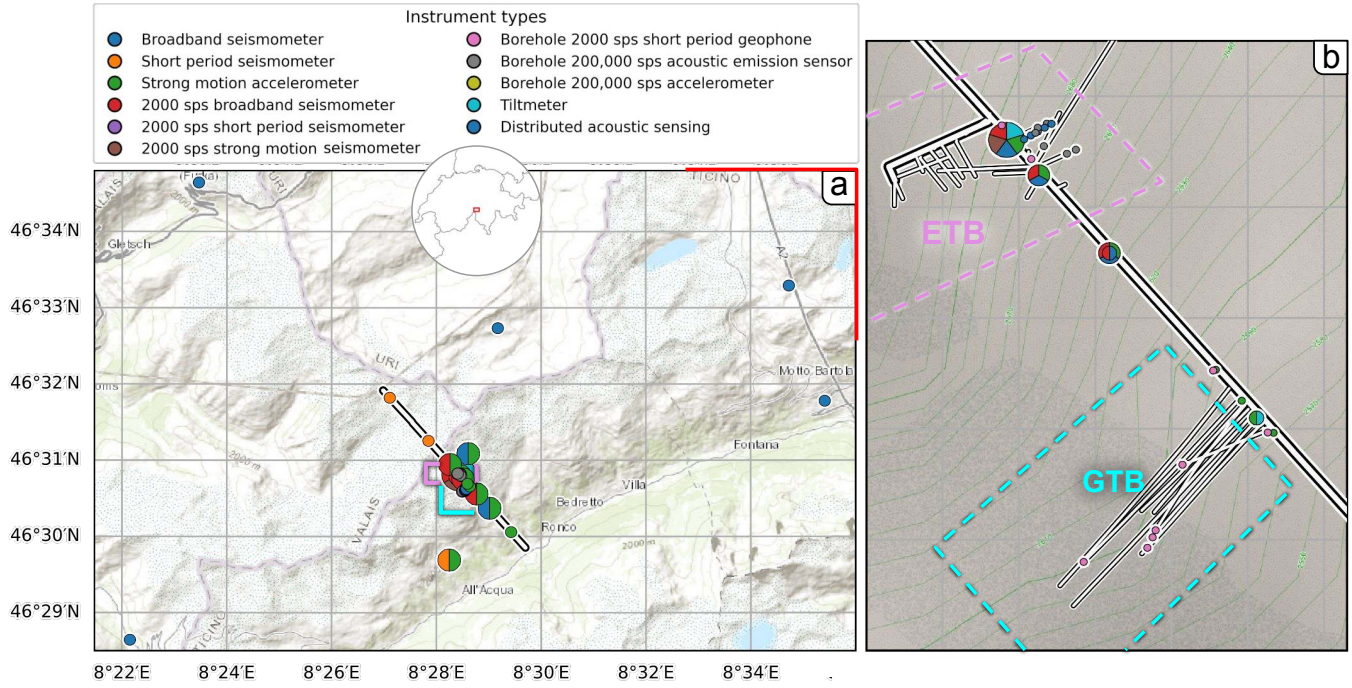

Figure 8 Overview of the seismic monitoring systems in and around the BedrettoLab. (a) Distribution of surface and tunnel stations forming the BULGG permanent network. (b) Seismic monitoring network around the two testbeds, including the selected borehole instruments that are included in the permanent monitoring system (see text for details). This figure has been made with Matplotlib (Hunter, 2007) and cartopy (Elson et al., 2024).

dynamic main shock slip episodes. The Earthquake Physics testbed infrastructure will facilitate fault activation and other fluid injection experiments during and beyond the FEAR project.

2.4 Experiments

The core of the FEAR project is a series of fault activation experiments where we simultaneously inject into the fault zone at multiple injection points, to activate specific fault segments (Figure 1). The core experiments began in November 2024 and are scheduled to run until August 2027.

2.4.1 Preparatory experiments (prior to FEAR)

Since July 2022, we have been conducting a series of preparatory test experiments, both at the target fault zone in the nascent Earthquake Physics Testbed, and at the Geoenergies Testbed, which is located approximately 400 metres to the South-East (Figure 1).

In the course of the Validating of Technologies for Reservoir Engineering (VALTER) project (Bröker et al., 2024a; Giardini et al., 2022; Ma et al., 2022; Plenkers et al., 2023), a series of 14 fluid injection experiments was performed in the Geoenergies Testbed. These tests utilized a multi-packer zonal isolation system that facilitates the injection of fluids into 8 different intervals of a single borehole at pressures ranging from 9.6 to 24.4 MPa and flow rates between 3 and 200 l/min. Injections with volumes between 1 m^3 to ~274 m^3 led to the seismic activation of a distributed fault and fracture systems, with over 40,000 locatable seismic events of magnitudes M_w -5.0 to -1.6 (Obermann et al., 2024). Seismic clouds highlighted activated structures reaching up to 100 metres in length. They are sub-parallel to the FEAR target fault zone (Figure 3c), which is ~400 m to the North West, in the Earthquake Physics Testbed, as well as to dominant structures mapped at the exposed on outcrop surfaces above the BedrettoLab (Ceccato et al., 2023). Selected experiments in the VALTER project were designed to test injection protocol ideas for FEAR (internally referred to as "VALTER-for-FEAR", and labelled as "V4F" in Figure 7). The technological developments in VALTER, specifically related to the multi-disciplinary and multi-scale monitoring systems (Plenkers et al., 2023), are directly transferable to the deployment of sensors in the Earthquake Physics Testbed (Figure 5).

During the Stress Profiling in Enhanced Geothermal Systems (SPINE) campaign conducted in December 2022 (Bröker et al., 2025b,a), we performed first small volume (0.14-0.60 m^3) injections into the FEAR target fault zone, on the north-west side of the Bedretto tunnel (Figures 1 & 5), using a SIMFIP probe. These experiments confirmed that we can induce at least small amplitude aseismic slip (up to 0.07 mm) on the target structure with fluid injections. Furthermore, stress inversions of SIMFIP injection experiments in separate borehole intervals above, inside, and below the MC fault zone suggest that up to 20 m from the target fault, principal stress axes are rotated by approximately 50° (Bröker et al., 2025b,a). Similar stress rotations have been hypothesized to occur approaching fault structures in larger tectonic settings due fractured damage zone surrounding faults (Faulkner et al., 2006).

During the excavation of the 110 m long FEAR tunnel between July 2024 and May 2025, an 11 m long tunnel

section (between tunnel metres 10 - 21) was excavated using the "Line Drilling and Rock Breaking" method (referred to informally as "soft excavation"), instead of the more conventional drill-and-blast method. This involved drilling a series of boreholes along the tunnel perimeter and removing the inner section by breaking the rock with a rock splitter. The objective was to investigate the development of the Excavation Damage Zone (EDZ) purely as a result of stress redistribution, while minimizing construction-induced damage typically caused by drill-and-blast techniques (Hamdi et al., 2024). The MC fault zone was monitored with a DORSA system during part of the soft-excavation (12.5 m–21 m) and subsequent drill-and-blast (21 m to 110 m), and it did not show any measurable slip due to the excavation. This project, termed PreCode, offers insights into fault zone activation by tunnelling.

2.4.2 Mzero experiments

In the "Mzero" experiments we used the existing experiment infrastructure of the Geoenergies Testbed and attempted to trigger M_w~0.0 quakes (Meier et al., 2025). This is substantially smaller than the FEAR target magnitude (M_w~1.0), but a significant step towards it, in that it is much higher than the largest events so far triggered in the VALTER experiments (M_w -1.6). We performed two major injection experiments in which we re-stimulated volumes which had already been stimulated in the VALTER project (Obermann et al., 2024). These were the first experiments at the BedrettoLab where we used the remote experiment control system (Section 2.3). Without the need for any personnel in the tunnel, this system enabled injections with higher flow rates, pressure, and injected volumes. The primary goal of the experiments was to investigate if we can amplify the seismogenic response of the rock mass using tailored injection protocols to increase the probability of a M_w ~ 0.0 event.

During the "MzeroA" experiment in April–May 2024, we injected a total of 84 m^3 of water over the course of 16 h, to hydraulically pre-condition major fractures in the volume. This strategy consisted of a first stage with an injection at a constant, intermediate injection pressure of 15.0 MPa for 4.5 days (59 m^3 injected volume) which was slightly below the jacking pressure (15.5 MPa) as determined from previous Hydraulic Tests on Pre-existing Fractures (HTPF). This sequence produced low levels of seismicity, averaging rates of only 3–4 detected events per hour. In the second stage, we raised injection pressures to 20 MPa, and in response seismicity rates increased to > 400 events per hour on average.

During the "MzeroB" experiment in August 2024, we began with a repetition of the high-pressure injection stage of the MzeroA experiment within the same interval, but without a pre-conditioning stage. The resulting seismicity rate was 4-5 times as high (80-100 events/min) as in the MzeroA experiment. Here, we upheld the 20 MPa stimulation for a total of 70 hours, injecting a total of 147 m^3.

The two Mzero experiments were much larger than any of the previous injection experiments at the Geoenergies Testbed: a total of 270 m^3 was injected. This is almost 20 times the previously injected volumes (14.4 m^3) in interval 11 (Obermann et al., 2024). These tests offer a first perspective on how injection protocols may be used to trigger larger magnitude events on a natural fault and fracture network. In addition, the experiments also revealed the full potential of the experimental setup. The ultra-broadband seismic network in the Geoenergies Testbed located ~54,000 seismic events with M_w -4.9 to -0.5. Because of the relatively short source-receiver distances, the seismic waveforms are almost unaffected by anelastic attenuation, which facilitates kinematic characterisations of the largest events through probabilistic spectral inversions (Supino et al., 2019). The observations made in the Mzero experiments played a crucial role in the design of the core FEAR experiments at the Earthquake Physics Testbed, in which we inject directly into the target fault, via multiple injection points simultaneously, to trigger and study the M_w ~1.0 target events.

2.4.3 Experiments on the target fault zone

In the "FEAR-1" experiment (November–December 2024), we performed the first large injection into the target fault zone, on the north-east side of the Bedretto tunnel (Figures 1 & 5), before the FEAR tunnel and the Earthquake Physics Testbed were completed. The goal was to induce aseismic slip on the order of a few millimetres, without triggering a larger dynamic rupture. A primary aim was to characterise the hydraulic, hydromechanical, and seismic response of the target fault zone to stimulation in a safe manner.

In a series of 14 injection tests, we injected a total of ~1,000 m^3 of water. In this experiment, two SIMFIP probes were deployed in two separated fault-crossing boreholes. We triggered and located 9,000 seismic events both on and off the main fault structures. The SIMFIP measurements at the injection points, as well as the off-fault strain observations, suggest that the target fault was indeed aseismically activated, along with prominent intersecting secondary structures.

2.4.4 Planned experiments

Upon completion of the experimental setup, the main FEAR experiments will be performed on the south-west part of the Earthquake Physics Testbed where the new FEAR tunnel is located (Figure 1). We will likely utilize a staggered fluid injection approach, via the injection boreholes, in an attempt to trigger a dynamic main shock rupture with a target size of M_w~1.0. If we are successful in triggering a rupture of substantial size, we will attempt to activate adjacent fault zone segments, to study how they have been affected by the first rupture. That is, after a potential additional drilling and instrumentation campaign to densify the monitoring, we will attempt to trigger more M_w~1.0 sized events directly where co- and post-seismic deformation may have raised stresses, but where the first rupture had for some reason stopped. With the experience gained from these experiments we may then attempt to actively

condition individual fault zone segments, e.g. with advanced injection protocols, in order to promote or prevent dynamic ruptures of particular segments, and to influence the rupture style, e.g. from seismic to more aseismic deformation.

2.5 Safety and risk

A principal risk associated with this project, and with stimulation experiments in the Bedretto tunnel more broadly, arises from ground motions generated by induced seismicity. Even low-magnitude events (M_w~1.0) that are not perceptible at the ground surface above the tunnel can produce large near-field peak ground accelerations (PGA) within tens of metres of the hypocentre, potentially sufficient to damage the tunnel walls. In the FEAR experimental design, we deliberately selected a fault considered reactivatable. The fault zone extent has been traced to at least 200 metres (Section 2.2). Furthermore, we will attempt to pre-condition it to promote rupture. While our target scenario is a dynamic mainshock of approximately M_w 1.0, the present uncertainties in rupture nucleation, propagation, and arrest—the very motivation for FEAR—imply a distinct probability that the rupture could continue to propagate and grow to $M_w \geq 1$. Accordingly, quantitative seismic risk assessment and mitigation measures are critical requirements, and informed the design at all stages of the experiment. This includes not only technical aspects but also a team culture with respect to risk, as well as the understanding that good risk management is a dynamic process and it should rely on several layers of safety.

Similar to hydraulic stimulation operations in large-scale geo-energy projects (e.g. Broccardo et al., 2020), induced-seismicity hazard analyses are performed prior to all hydraulic stimulation experiments at the BedrettoLab, following the procedure outlined by Gischig et al. (2025). As a first step, we compile an inventory of exposed elements (objects at risk), including:

i. Personnel, equipment, and the tunnel infrastructure within the experimental cavern and along the Bedretto tunnel (standoff distances ~10–300 m)

ii. Machinery in the machine room at the junction where the Bedretto tunnel branches from the Furka tunnel, as well as the MGB railway, associated infrastructure, travellers, and workers in the Furka tunnel (distance from the experiments ~2.5 km)

iii. Settlements and individuals in the Bedretto valley (surface impact; distances ~2–25 km)

The seismic hazard and risk assessment integrates seismicity datasets from prior BedrettoLab stimulations at the Geoenergies Testbed with global compilations. Specifically, the seismogenic index (or feedback) a_{fb}-value and Gutenberg-Richter b-values of various BedrettoLab and global datasets were used to extrapolate towards larger magnitudes. Greater weight was assigned to the site-specific BedrettoLab data. The ground-motion model calibrated to past BedrettoLab events is shown in Figure 9a, and probabilistic magnitude estimates are shown in Figure 9b. In general, peak ground velocities (PGV) ≥ 30 mm/s are expected to produce localized damage to the tunnel and installations (e.g. fracturing, rockfall), a level that can be attained by an event of M_w~1.0 at a distance of ~30 m. Ground motions are typically felt above 1 mm/s. Considering the calibrated ground-motion relations, we conclude that the highest risk pertains to personnel and equipment within the tunnel, since this shaking level is achievable for M_w~1 at near-field distances. In contrast, generating damage-level shaking at distances >2 km would require an event on the order of M_w~4, subject to model uncertainty.

As shown by Gischig et al. (2025), achieving a convergent a priori estimate of the probability of reaching a given magnitude (e.g. the FEAR target of M_w 1.0) is difficult in the absence of site-specific data on the seismogenic response within the Earthquake Physics Testbed volume. The probability estimate and its uncertainty shown in Figure 9b indicates that this probability cannot be tightly constrained. The grey shading denotes epistemic uncertainty (model and parameter uncertainty) and aleatory variability (natural randomness) in the probability estimates. This was derived using the weighted a_{fb}- and b-values derived from past Bedretto stimulations and global datasets (epistemic uncertainty), as well as the uncertainty associated with these parameters (aleatory uncertainty) in 10^5 realisations. The result of these realisations was converted into a probability density function represented by the grey shading. From this, the median and percentiles were derived. Given this uncertainty, we generally adopt a conservative risk procedure. To reduce personnel exposure, we implemented a fully remote-operation capability (Section 2.3), enabling stimulation and post-stimulation activities without personnel in the tunnel. A traffic-light system based on both event magnitude and ground motion is deployed. For example, for the experiments in the Geoenergies Testbed, upon exceeding either $M_w \geq 0.0$ or a peak ground velocity (PGV) of 2.5 mm/s (orange alert), the experiment was temporarily suspended and subjected to reassessment before resumption. These values were chosen to stop well below a damaging magnitude (M_w~1.0) and ground motion. The combination of the traffic-light system and the remote-operated pump circuit ensure residual risks within acceptable bounds despite uncertainties in seismic hazard forecasts. Subsequent experiments will adopt the same framework. The probabilistic hazard and risk analysis will be updated iteratively as additional site-specific datasets from experiments at the Earthquake Physics Testbed become available, with corresponding recalibration of models and adjustment of operational thresholds and procedures as warranted.

3 Discussion

One key motivation for the FEAR project is that state-of-the-art understanding of earthquake processes is strongly observation-limited. From strain localisation to fault dilation and to fault healing mechanisms, there are numerous aspects of earthquake mechanics that

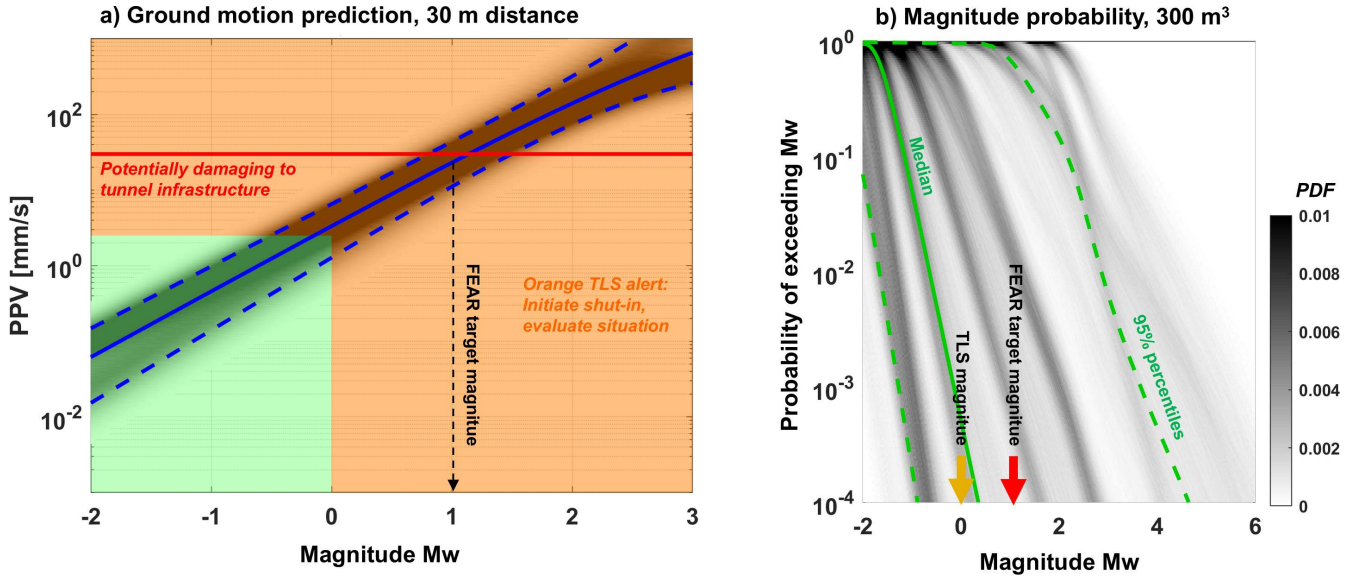

Figure 9 (a) Ground motion model calibrated against seismicity data from the BedrettoLab Geoenergies Testbed including uncertainty in grey shading. Solid blue line is the median and dashed blue lines the 90% percentiles. (b) Probability of exceeding a certain magnitude for an anticipated injected volume of 300 m^3. Grey shading is the probability density function (PDF) representing the aleatory and epistemic uncertainty of the predictions based on the Bedretto-specific and world-wide datasets. Green lines are the median and the percentiles derived from all possible predictions.

we cannot resolve with surface sensor networks, or even with near-fault observatories. To understand such first order phenomena in all their complexity, it may be necessary to build larger scale facilities that provide experimental control and extensive monitoring at very short recording distances, under in situ conditions. The Earthquake Physics Testbed we are building at the BedrettoLab is an attempt to build such a facility, where we can induce earthquakes of substantial size in the midst of monitoring arrays with high sensitivity and resolution. The Earthquake Physics Testbed may allow us to address a wide range of fundamental science and practical questions.

3.1 Science potential

One important example phenomenon that can profit from this larger scale in situ approach is precursory and rupture nucleation processes (Garagash and Germanovich, 2012; Ohnaka, 1992): small foreshock cascades and slow strain transients are often near—and possibly below—the detection limit of standard monitoring networks (e.g. Bletery and Nocquet, 2023; Obara and Kato, 2016; Socquet et al., 2017; Kato and Ben-Zion, 2020). While in laboratory experiments, precursory phenomena such as aseismic transients, localized foreshocks, and accelerated deformation prior to stick-slip or catastrophic brittle failure are commonly observed (Dieterich, 1979; McLaskey, 2019; Ohnaka, 2003; Selvadurai and Glaser, 2015; Xu et al., 2023), they are often absent in the data from before natural major earthquakes (Brodsky and Lay, 2014; Martínez-Garzón and Poli, 2024). It is unclear if these observations are ubiquitous to earthquakes, or are affected by the sparse coverage and distance in real tectonic settings or limitations of the sensing systems (Tullis, 1996).

3.2 Controlling induced seismicity

In order to understand how to prevent potentially damaging induced earthquakes during hydraulic stimulation, it may be helpful to first understand how we can trigger them. With the remote experiment control system and the BedrettoLab safety concept, we can study what it takes to trigger larger earthquakes, with somewhat bolder injection strategies than is usually possible in fluid injection experiments. This will provide the seismological community with rich datasets that are currently missing. With this, we can meaningfully test and compare the various proposed models for maximum earthquake size (Galis et al., 2017; McGarr, 2014; van der Elst et al., 2016). Furthermore, in some of the FEAR experiments we will attempt to directly condition different fault segments to either encourage or inhibit dynamic rupture. What are the relevant mechanisms for inducing fault slip, and can they be discerned (Moein et al., 2023)? For example, can we discern between triggered or driven induced events (Schultz et al., 2025)? Can we raise the critical nucleation size across the fault zone with slow, prolonged, and low-amplitude pressurisation, and thereby shift the total seismic moment balance from seismic to aseismic (Bentz et al., 2020)? Can we observe slower fault slip styles that are indicative of this transition? Can we effectively influence *i)* the fault area that is activated by seismicity; *ii)* the overall level of seismicity; *iii)* the size of the largest events; or iv) the relative proportion of small and large events? Can we hydro-mechanically clamp and shut down an individual fault segment that was previously slipping (Schultz, 2025)? Can we adequately anticipate the amount of trailing post-injection seismicity? Finally, are there practical ways to integrate these learnings into risk management strategies?

3.3 Predictability

The FEAR experiments are also a formidable opportunity to test the predictability of seismicity. In most natural seismic sequences, purely statistical models such as ETAS tend to outperform physics-based seismicity models. However, the Earthquake Physics Testbed setup provides much more information on the physical state of the target fault system than is usually available. Under such circumstances, can we construct a seismicity model which—contrary to standard models—makes higher probability gain statements on the location of individual events, or even on event magnitudes? Which attributes can we reliably forecast (e.g. seismicity rates, the spatial extent of the seismicity cloud, etc.), and which ones remain unpredictable? Furthermore, the experiments will also serve to test recent successful results from predictions of laboratory earthquakes at the in situ scale (Rouet-Leduc et al., 2017).

Ideally, we would be able to recognise the presence of loaded faults or fault segments prior to stimulation, e.g. in deep geothermal energy projects. If such faults were present, one could stay away from them, or carefully pressurize them to induce slow, aseismic slip that would relax the stresses that might otherwise lead to fast, damaging ruptures. An important practical question is therefore whether—given the level of observation and characterisation—we can recognise loaded, 'activatable' fault strands a priori. This could, for example, be possible because they would show diagnostic, observable patterns upon minor perturbations, such as systematic b-value variations (Gulia et al., 2016; Gulia and Wiemer, 2019; Tormann et al., 2014, 2015), or a decrease in the fraction of non-clustered seismicity (Ben-Zion and Zaliapin, 2020). The FEAR monitoring system will allow us to systematically search for diagnostic patterns, that may be unnoticeable with today's standard observatories.

4 Conclusions

The FEAR project is a bold initiative to advance our understanding of earthquake physics, by activating a natural fault zone in the Swiss Alps, in an experimental testbed that facilitates exceptional experiment control and monitoring. The project is designed *i)* to bridge the gap between the laboratory and natural scales: our monitoring conditions are similar to those in a rock mechanics laboratory, but we experiment in a natural setting, with real fault zone structures and corresponding natural stress fields; *ii)* to bridge scientific domains, by combining all major observables that are relevant for earthquake faulting processes, including geology, seismology and hydromechanics; and *iii)* to bridge scientific approaches, via the integration of in situ experiments, accompanying rock mechanics laboratory experiments, and numerical process models. With the direct fault zone access the BedrettoLab provides, the FEAR project may be able to advance our understanding of what it takes to trigger—and, more importantly, to prevent—larger quakes in fluid injection experiments. It may also shed new light on a wide range of questions on earthquake precursors, predictability, and rupture dynamics, and on how to effectively manage seismic risk.

Acknowledgements

We would like to thank editor Ake Fagereng, reviewer John Vidale, and one anonymous reviewer for their constructive comments and suggestions in the review process. We highly appreciate the valuable feedback we receive from Bill Ellsworth, Jean-Paul Ampuero, Daniel Faulkner, Marco Herwegh, Chris Marone, Michel Campillo, and Inga Berre in their function as members of the external advisory board of the FEAR project. Furthermore, we are grateful to the numerous people that work 'behind the curtains' to make the BedrettoLab and FEAR experiments possible, including Bekir Yuece, Erminio Molteni, Marco Bertoldi, and many more. We thank Simone Zaugg for the design work of Figure 1. The FEAR project is funded by the European Research Council (ERC) project FEAR (grant 856559) under the European Union's Horizon 2020 research and innovation program. The BedrettoLab is financed by the Werner Siemens Foundation, ETH Zürich, and the Swiss National Science Foundation.

Data and code availability

The collected data sets from the FEAR experiments will be openly accessible after an embargo period of 24 months from the end of data collection, or earlier if the corresponding scientific publication is released before the embargo ends. For all major FEAR experiments, we are planning to provide a metadata-only publication with a comprehensive list of all data sets acquired, and with instructions on how to access and use the data. The corresponding data report for the FEAR-1 experiment is in preparation and will be available from the ETHZ data repository, DOI: 10.3929/ethz-c-000783939. Seismic network products such as station metadata, seismic data, and seismic event catalogues will be available through the International Federation of Digital Seismograph Networks (FDSN) webservices, hosted by the Swiss Seismological Service (SED) at ETH Zürich, via the BULGG seismic network, Switzerland (Bedretto Lab), DOI: 10.12686/SED/NETWORKS/8R.

Competing interests

The authors declare no competing interests.

References

Aben, F. M. and Brantut, N. Dilatancy stabilises shear failure in rock. *Earth and Planetary Science Letters*, 574:117174, Nov. 2021. doi: 10.1016/j.epsl.2021.117174.

Abercrombie, R. E. Resolution and uncertainties in estimates of earthquake stress drop and energy release. *Philosophical Transactions of the Royal Society A: Mathematical, Physical and Engineering Sciences*, 379(2196):20200131, Mar. 2021. doi: 10.1098/rsta.2020.0131.

Abercrombie, R. E. and Rice, J. R. Can observations of earthquake scaling constrain slip weakening? *Geophysical Journal International*, 162(2):406–424, Aug. 2005. doi: 10.1111/j.1365-246x.2005.02579.x.

Abercrombie, R. E., Baltay, A., Chu, S., Taira, T., Bindi, D., Boyd, O. S., Chen, X., Cochran, E. S., Devin, E., Dreger, D., Ellsworth, W., Fan, W., Harrington, R. M., Huang, Y., Kemna, K. B., Liu, M., Oth, A., Parker, G. A., Pennington, C., Picozzi, M., Ruhl, C. J., Shearer, P., Spallarossa, D., Trugman, D., Vandevert, I., Wu, Q., Yoon, C., Yu, E., Beroza, G. C., Eulenfeld, T., Knudson, T., Mayeda, K., Morasca, P., Neely, J. S., Roman-Nieves, J., Satriano, C., Supino, M., Walter, W. R., Archuleta, R., Atkinson, G. M., Calderoni, G., Ji, C., Yang, H., and Zhang, J. Overview of the SCEC/USGS Community Stress Drop Validation Study Using the 2019 Ridgecrest Earthquake Sequence. *Bulletin of the Seismological Society of America*, 115(3):734–759, May 2025. doi: 10.1785/0120240158.

Achtziger-Zupančič, P., Ceccato, A., Zappone, A. S., Pozzi, G., Shakas, A., Amann, F., Behr, W. M., Escallon Botero, D., Giardini, D., Hertrich, M., Jalali, M., Ma, X., Meier, M.-A., Osten, J., Wiemer, S., and Cocco, M. Selection and Characterisation of the Target Fault for Fluid-Induced Activation and Earthquake Rupture Experiments. Mar. 2024. doi: 10.5194/egusphere-2024-586.

Aki, K. Characterization of barriers on an earthquake fault. *Journal of Geophysical Research: Solid Earth*, 84(B11):6140–6148, Oct. 1979. doi: 10.1029/jb084ib11p06140.

Aki, K. Asperities, barriers, characteristic earthquakes and strong motion prediction. *Journal of Geophysical Research: Solid Earth*, 89(B7):5867–5872, July 1984. doi: 10.1029/jb089ib07p05867.

Aretusini, S., Nuñez Cascajero, A., Cornelio, C., Barrero Echevarria, X., Spagnuolo, E., Tapetado, A., Vazquez, C., Di Toro, G., and Cocco, M. Mechanical Energy Dissipation During Seismic Dynamic Weakening in Calcite-Bearing Faults. *Journal of Geophysical Research: Solid Earth*, 129(9), Sept. 2024. doi: 10.1029/2024jb028927.

Baltay, A., Abercrombie, R., Chu, S., and Taira, T. The SCEC/USGS Community Stress Drop Validation Study Using the 2019 Ridgecrest Earthquake Sequence. *Seismica*, 3(1), May 2024. doi: 10.26443/seismica.v3i1.1009.

Barbot, S., Lapusta, N., and Avouac, J.-P. Under the Hood of the Earthquake Machine: Toward Predictive Modeling of the Seismic Cycle. *Science*, 336(6082):707–710, May 2012. doi: 10.1126/science.1218796.

Behr, W. M. and Bürgmann, R. What's down there? The structures, materials and environment of deep-seated slow slip and tremor. *Philosophical Transactions of the Royal Society A: Mathematical, Physical and Engineering Sciences*, 379(2193): 20200218, Feb. 2021. doi: 10.1098/rsta.2020.0218.

Ben-Zion, Y. and Sammis, C. G. Characterization of Fault Zones. *Pure and Applied Geophysics*, 160(3):677–715, Mar. 2003. doi: 10.1007/pl00012554.

Ben-Zion, Y. and Zaliapin, I. Localization and coalescence of seismicity before large earthquakes. *Geophysical Journal International*, 223(1):561–583, June 2020. doi: 10.1093/gji/ggaa315.

Bentz, S., Kwiatek, G., Martínez-Garzón, P., Bohnhoff, M., and Dresen, G. Seismic Moment Evolution During Hydraulic Stimulations. *Geophysical Research Letters*, 47(5), Mar. 2020. doi: 10.1029/2019gl086185.

Ben-Zion, Y. Collective behavior of earthquakes and faults: Continuum-discrete transitions, progressive evolutionary changes, and different dynamic regimes. *Reviews of Geophysics*, 46(4), Dec. 2008. doi: 10.1029/2008rg000260.

Beroza, G. C. and Ide, S. Slow Earthquakes and Nonvolcanic Tremor. *Annual Review of Earth and Planetary Sciences*, 39 (1):271–296, May 2011. doi: 10.1146/annurev-earth-040809-152531.

Blanke, A., Boese, C. M., Dresen, G., Bohnhoff, M., and Kwiatek, G. Metre-scale damage zone characterization usingS-coda waves from active ultrasonic transmission measurements in the STIMTEC project, URL Reiche Zeche, Germany. *Geophysical Journal International*, 233(2):1339–1355, Jan. 2023. doi: 10.1093/gji/ggad003.

Bletery, Q. and Nocquet, J.-M. The precursory phase of large earthquakes. *Science*, 381(6655):297–301, July 2023. doi: 10.1126/science.adg2565.

Boese, C. M., Kwiatek, G., Fischer, T., Plenkers, K., Starke, J., Blümle, F., Janssen, C., and Dresen, G. Seismic monitoring of the STIMTEC hydraulic stimulation experiment in anisotropic metamorphic gneiss. *Solid Earth*, 13(2):323–346, Feb. 2022. doi: 10.5194/se-13-323-2022.

Bohnhoff, M., Dresen, G., Ellsworth, W. L., and Ito, H. *Passive Seismic Monitoring of Natural and Induced Earthquakes: Case Studies, Future Directions and Socio-Economic Relevance*, page 261–285. Springer Netherlands, 2009. doi: 10.1007/978-90-481-2737-5_7.

Bouchon, M., Karabulut, H., Aktar, M., Özalaybey, S., Schmittbuhl, J., and Bouin, M.-P. Extended Nucleation of the 1999 Mw 7.6 Izmit Earthquake. *Science*, 331(6019):877–880, Feb. 2011. doi: 10.1126/science.1197341.

Brantut, N. Dilatancy-induced fluid pressure drop during dynamic rupture: Direct experimental evidence and consequences for earthquake dynamics. *Earth and Planetary Science Letters*, 538: 116179, May 2020. doi: 10.1016/j.epsl.2020.116179.

Brennwald, M. S., Schmidt, M., Oser, J., and Kipfer, R. A Portable and Autonomous Mass Spectrometric System for On-Site Environmental Gas Analysis. *Environmental Science & Technology*, 50(24):13455–13463, Dec. 2016. doi: 10.1021/acs.est.6b03669.

Broccardo, M., Mignan, A., Grigoli, F., Karvounis, D., Rinaldi, A. P., Danciu, L., Hofmann, H., Milkereit, C., Dahm, T., Zimmermann, G., Hjörleifsdóttir, V., and Wiemer, S. Induced seismicity risk analysis of the hydraulic stimulation of a geothermal well on Geldinganes, Iceland. *Natural Hazards and Earth System Sciences*, 20(6):1573–1593, June 2020. doi: 10.5194/nhess-20-1573-2020.

Brodsky, E. E. and Lay, T. Recognizing Foreshocks from the 1 April 2014 Chile Earthquake. *Science*, 344(6185):700–702, May 2014. doi: 10.1126/science.1255202.

Brodsky, E. E., Kirkpatrick, J. D., and Candela, T. Constraints from fault roughness on the scale-dependent strength of rocks. *Geology*, 44(1):19–22, Nov. 2015. doi: 10.1130/g37206.1.

Brune, J. N. Tectonic stress and the spectra of seismic shear waves from earthquakes. *Journal of Geophysical Research*, 75(26): 4997–5009, Sept. 1970. doi: 10.1029/jb075i026p04997.

Bröker, K. and Ma, X. Estimating the Least Principal Stress in a Granitic Rock Mass: Systematic Mini-Frac Tests and Elaborated Pressure Transient Analysis. *Rock Mechanics and Rock Engineering*, 55(4):1931–1954, Jan. 2022. doi: 10.1007/s00603-021-02743-1.

Bröker, K., Ma, X., Gholizadeh Doonechaly, N., Rosskopf, M., Obermann, A., Rinaldi, A. P., Hertrich, M., Serbeto, F., Maurer, H., Wiemer, S., and Giardini, D. Hydromechanical characterization of a fractured crystalline rock volume during multi-stage hydraulic stimulations at the BedrettoLab. *Geothermics*, 124: 103126, Dec. 2024a. doi: 10.1016/j.geothermics.2024.103126.

Bröker, K., Ma, X., Zhang, S., Gholizadeh Doonechaly, N., Hertrich, M., Klee, G., Greenwood, A., Caspari, E., and Giardini, D. Constraining the stress field and its variability at the BedrettoLab: Elaborated hydraulic fracture trace analysis. *International Journal of Rock Mechanics and Mining Sciences*, 178:105739, June

2024b. doi: 10.1016/j.ijrmms.2024.105739.

Bröker, K., Guglielmi, Y., Soom, F., Cook, P., Hertrich, M., and Valley, B. In situ quantification of fracture slip induced by hydraulic injections in a deep borehole: A comparison of two different borehole techniques. Unpublished, Submitted to IJRMMS, 2025a. doi: 10.2139/ssrn.5967430.

Bröker, K., Valley, B., Soom, F., Cook, P., Guigliemi, Y., and Hertrich, M. Stress field characterisation from fracture slip inversion at the BedrettoLab. European Geothermal Congress, 2025b. https://europeangeothermalcongress.eu/wp-content/uploads/2025/11/Kai-et-al.pdf.

Bürgmann, R. The geophysics, geology and mechanics of slow fault slip. *Earth and Planetary Science Letters*, 495:112–134, Aug. 2018. doi: 10.1016/j.epsl.2018.04.062.

Caine, J. S., Evans, J. P., and Forster, C. B. Fault zone architecture and permeability structure. *Geology*, 24(11):1025, 1996. doi: 10.1130/0091-7613(1996)024<1025:fzaaps>2.3.co;2.

Candela, T., Renard, F., Bouchon, M., Brouste, A., Marsan, D., Schmittbuhl, J., and Voisin, C. Characterization of Fault Roughness at Various Scales: Implications of Three-Dimensional High Resolution Topography Measurements. *Pure and Applied Geophysics*, 166(10–11):1817–1851, June 2009. doi: 10.1007/s00024-009-0521-2.

Candela, T., Renard, F., Bouchon, M., Schmittbuhl, J., and Brodsky, E. E. Stress Drop during Earthquakes: Effect of Fault Roughness Scaling. *Bulletin of the Seismological Society of America*, 101(5): 2369–2387, Sept. 2011. doi: 10.1785/0120100298.

Cappa, F., Scuderi, M. M., Collettini, C., Guglielmi, Y., and Avouac, J.-P. Stabilization of fault slip by fluid injection in the laboratory and in situ. *Science Advances*, 5(3), Mar. 2019. doi: 10.1126/sciadv.aau4065.

Cattania, C. and Segall, P. Precursory Slow Slip and Foreshocks on Rough Faults. *Journal of Geophysical Research: Solid Earth*, 126 (4), Apr. 2021. doi: 10.1029/2020jb020430.

Ceccato, A., Behr, W. M., Zappone, A., Tavazzani, L., and Giuliani, A. Structural evolution, exhumation rates, and rheology of the European crust during Alpine collision: constraints from the Rotondo granite - Gotthard nappe. Dec. 2023. doi: 10.22541/au.170293691.11620931/v1.

Ceccato, A., Behr, W. M., Zappone, A. S., Tavazzani, L., and Giuliani, A. Structural Evolution, Exhumation Rates, and Rheology of the European Crust During Alpine Collision: Constraints From the Rotondo Granite—Gotthard Nappe. *Tectonics*, 43(6), June 2024. doi: 10.1029/2023tc008219.

Chester, F. M., Evans, J. P., and Biegel, R. L. Internal structure and weakening mechanisms of the San Andreas Fault. *Journal of Geophysical Research: Solid Earth*, 98(B1):771–786, Jan. 1993. doi: 10.1029/92jb01866.

Cicerone, R. D., Ebel, J. E., and Britton, J. A systematic compilation of earthquake precursors. *Tectonophysics*, 476(3–4):371–396, Oct. 2009. doi: 10.1016/j.tecto.2009.06.008.

Cocco, M., Tinti, E., and Cirella, A. On the scale dependence of earthquake stress drop. *Journal of Seismology*, 20(4): 1151–1170, July 2016. doi: 10.1007/s10950-016-9594-4.

Cocco, M., Aretusini, S., Cornelio, C., Nielsen, S. B., Spagnuolo, E., Tinti, E., and Di Toro, G. Fracture Energy and Breakdown Work During Earthquakes. *Annual Review of Earth and Planetary Sciences*, 51(1):217–252, May 2023. doi: 10.1146/annurev-earth-071822-100304.

Collettini, C., Carpenter, B., Viti, C., Cruciani, F., Mollo, S., Tesei, T., Trippetta, F., Valoroso, L., and Chiaraluce, L. Fault structure and slip localization in carbonate-bearing normal faults: An example from the Northern Apennines of Italy. *Journal of Structural Geology*, 67:154–166, Oct. 2014. doi: 10.1016/j.jsg.2014.07.017.

Colombelli, S., Zollo, A., Festa, G., and Picozzi, M. Evidence for a difference in rupture initiation between small and large earthquakes. *Nature Communications*, 5(1), June 2014. doi: 10.1038/ncomms4958.

Conti, L., Picozza, P., and Sotgiu, A. A Critical Review of Ground Based Observations of Earthquake Precursors. *Frontiers in Earth Science*, 9, July 2021. doi: 10.3389/feart.2021.676766.

Cornelio, C., Aretusini, S., Spagnuolo, E., Di Toro, G., and Cocco, M. Multiple Seismic Slip-Rate Pulses and Mechanical and Textural Evolution of Calcite-Bearing Fault Gouges. *Journal of Geophysical Research: Solid Earth*, 129(7), July 2024. doi: 10.1029/2024jb029099.

Derode, B., Guglielmi, Y., De Barros, L., and Cappa, F. Seismic responses to fluid pressure perturbations in a slipping fault. *Geophysical Research Letters*, 42(9):3197–3203, May 2015. doi: 10.1002/2015gl063671.

De Barros, L., Guglielmi, Y., Cappa, F., Nussbaum, C., and Birkholzer, J. Induced microseismicity and tremor signatures illuminate different slip behaviours in a natural shale fault reactivated by a fluid pressure stimulation (Mont Terri). *Geophysical Journal International*, 235(1):531–541, May 2023. doi: 10.1093/gji/ggad231.

Di Toro, G., Niemeijer, A., Tripoli, A., Nielsen, S., Di Felice, F., Scarlato, P., Spada, G., Alessandroni, R., Romeo, G., Di Stefano, G., Smith, S., Spagnuolo, E., and Mariano, S. From field geology to earthquake simulation: a new state-of-the-art tool to investigate rock friction during the seismic cycle (SHIVA). *RENDICONTI LINCEI*, 21(S1):95–114, Oct. 2010. doi: 10.1007/s12210-010-0097-x.

Di Toro, G., Han, R., Hirose, T., De Paola, N., Nielsen, S., Mizoguchi, K., Ferri, F., Cocco, M., and Shimamoto, T. Fault lubrication during earthquakes. *Nature*, 471(7339):494–498, Mar. 2011. doi: 10.1038/nature09838.

Diehl, T., Clinton, J., Cauzzi, C., Kraft, T., Kästli, P., Deichmann, N., Massin, F., Grigoli, F., Molinari, I., Böse, M., Hobiger, M., Haslinger, F., Fäh, D., and Wiemer, S. Earthquakes in Switzerland and surrounding regions during 2017 and 2018. *Swiss Journal of Geosciences*, 114(1), Feb. 2021. doi: 10.1186/s00015-020-00382-2.

Diehl, T., Cauzzi, C., Clinton, J., Kraft, T., Kästli, P., Massin, F., Lanza, F., Simon, V., Grigoli, F., Hobiger, M., Roth, P., Haslinger, F., Fäh, D., and Wiemer, S. Earthquakes in Switzerland and surrounding regions during 2019 and 2020. *Swiss Journal of Geosciences*, 118 (1), July 2025. doi: 10.1186/s00015-025-00489-4.

Dieterich, J. H. Preseismic fault slip and earthquake prediction. *Journal of Geophysical Research: Solid Earth*, 83(B8):3940–3948, Aug. 1978. doi: 10.1029/jb083ib08p03940.

Dieterich, J. H. Modeling of rock friction: 1. Experimental results and constitutive equations. *Journal of Geophysical Research: Solid Earth*, 84(B5):2161–2168, May 1979. doi: 10.1029/jb084ib05p02161.

Dieterich, J. H. and Kilgore, B. D. Direct observation of frictional contacts: New insights for state-dependent properties. *pure and applied geophysics*, 143(1–3):283–302, Mar. 1994. doi: 10.1007/bf00874332.

Dragert, H., Wang, K., and James, T. S. A Silent Slip Event on the Deeper Cascadia Subduction Interface. *Science*, 292(5521): 1525–1528, May 2001. doi: 10.1126/science.1060152.

Dutler, N. O., Valley, B., Amann, F., Jalali, M., Villiger, L., Krietsch, H., Gischig, V., Doetsch, J., and Giardini, D. Poroelasticity Contributes to Hydraulic-Stimulation Induced Pressure Changes. *Geophysical Research Letters*, 48(6), Mar. 2021. doi: 10.1029/2020gl091468.

Ellsworth, W., Hickman, S., Zoback, M., Imanishi, K., Thurber, C., and Roecker, S. Micro-nano-and picoearthquakes at SAFOD: Implications for earthquake rupture and fault mechanics. In *AGU Fall Meeting Abstracts*, page 12 –05, 2007.

Ellsworth, W. L. and Beroza, G. C. Seismic Evidence for an Earthquake Nucleation Phase. *Science*, 268(5212):851–855, May 1995. doi: 10.1126/science.268.5212.851.

Elson, P., de Andrade, E. S., Lucas, G., May, R., Hattersley, R., Campbell, E., Comer, R., Dawson, A., Little, B., Raynaud, S., scmc72, Snow, A. D., lgolston, Blay, B., Killick, P., lbdreyer, Peglar, P., Wilson, N., Andrew, Szymaniak, J., Berchet, A., Bosley, C., Davis, L., Filipe, Krasting, J., Bradbury, M., Worsley, S., and Kirkham, D. SciTools/cartopy: v0.21.0, Zenodo, 2024. doi: 10.5281/ZENODO.1182735.

Faulkner, D., Jackson, C., Lunn, R., Schlische, R., Shipton, Z., Wibberley, C., and Withjack, M. A review of recent developments concerning the structure, mechanics and fluid flow properties of fault zones. *Journal of Structural Geology*, 32(11):1557–1575, Nov. 2010. doi: 10.1016/j.jsg.2010.06.009.

Faulkner, D. R., Mitchell, T. M., Healy, D., and Heap, M. J. Slip on "weak" faults by the rotation of regional stress in the fracture damage zone. *Nature*, 444(7121):922–925, Dec. 2006. doi: 10.1038/nature05353.

Frank, F. C. On dilatancy in relation to seismic sources. *Reviews of Geophysics*, 3(4):485–503, Nov. 1965. doi: 10.1029/rg003i004p00485.

Galis, M., Ampuero, J. P., Mai, P. M., and Cappa, F. Induced seismicity provides insight into why earthquake ruptures stop. *Science Advances*, 3(12), Dec. 2017. doi: 10.1126/sciadv.aap7528.

Garagash, D. I. and Germanovich, L. N. Nucleation and arrest of dynamic slip on a pressurized fault. *Journal of Geophysical Research: Solid Earth*, 117(B10), Oct. 2012. doi: 10.1029/2012jb009209.

Giardini, D., Wiemer, S., Maurer, H., Hertrich, M., Meier, P., Alcolea, A., Castilla, R., and Hochreutener, R. Validation of Technologies for reservoir engineering (VALTER). Technical report, 2022. doi: 10.3929/ETHZ-B-000644092.

Gibowicz, S. and Kijko, A. *An introduction to mining seismology*. Academic press, 1994.

Gischig, V. S., Rinaldi, A. P., Alcolea, A., Bethman, F., Broccardo, M., Bröker, K. E. N., Castilla, R., Ciardo, F., Clasen Repollés, V., Durand, V., Gholizadeh Doonechaly, N., Hertrich, M., Hochreutener, R., Kästli, P., Karvounis, D., Ma, X., Meier, M.-A., Meier, P., Mesimeri, M., Mignan, A., Obermann, A., Plenkers, K., Rosskopf, M., Serbeto, F., Selvadurai, P. A., Shakas, A., Villiger, L., Wenning, Q., Zappone, A., Aaron, J., Maurer, H., and Giardini, D. Updating induced seismic hazard assessments during hydraulic stimulation experiments in underground laboratories: workflow and limitations. Jan. 2025. doi: 10.5194/egusphere-2024-3882.

Goebel, T. H. W. and Brodsky, E. E. The spatial footprint of injection wells in a global compilation of induced earthquake sequences. *Science*, 361(6405):899–904, Aug. 2018. doi: 10.1126/science.aat5449.

Goebel, T. H. W., Becker, T. W., Schorlemmer, D., Stanchits, S., Sammis, C., Rybacki, E., and Dresen, G. Identifying fault heterogeneity through mapping spatial anomalies in acoustic emission statistics. *Journal of Geophysical Research: Solid Earth*, 117 (B3), Mar. 2012. doi: 10.1029/2011jb008763.

Goebel, T. H. W., Becker, T. W., Sammis, C. G., Dresen, G., and Schorlemmer, D. Off-fault damage and acoustic emission distributions during the evolution of structurally complex faults over series of stick-slip events. *Geophysical Journal International*, 197 (3):1705–1718, Apr. 2014. doi: 10.1093/gji/ggu074.

Goebel, T. H. W., Schuster, V., Kwiatek, G., Pandey, K., and Dresen, G. A laboratory perspective on accelerating preparatory processes before earthquakes and implications for foreshock detectability. *Nature Communications*, 15(1), July 2024. doi: 10.1038/s41467-024-49959-7.

Goldsby, D. L. and Tullis, T. E. Flash Heating Leads to Low Frictional Strength of Crustal Rocks at Earthquake Slip Rates. *Science*, 334 (6053):216–218, Oct. 2011. doi: 10.1126/science.1207902.

Grigoli, F., Cesca, S., Rinaldi, A. P., Manconi, A., López-Comino, J. A., Clinton, J. F., Westaway, R., Cauzzi, C., Dahm, T., and Wiemer, S. The November 2017 M w 5.5 Pohang earthquake: A possible case of induced seismicity in South Korea. *Science*, 360(6392): 1003–1006, June 2018. doi: 10.1126/science.aat2010.

Guglielmi, Y., Cappa, F., Rutqvist, J., Tsang, C., Wang, J., Lançon, H., Durand, J., and Janowczyk, J. Step-Rate Injection Method for Fracture In-Situ Properties (SIMFIP): Monitoring Fractures Stimulation Efficiency. ARMA-2014-7505., 2014.

Guglielmi, Y., Cappa, F., Avouac, J.-P., Henry, P., and Elsworth, D. Seismicity triggered by fluid injection–induced aseismic slip. *Science*, 348(6240):1224–1226, June 2015a. doi: 10.1126/science.aab0476.

Guglielmi, Y., Elsworth, D., Cappa, F., Henry, P., Gout, C., Dick, P., and Durand, J. In situ observations on the coupling between hydraulic diffusivity and displacements during fault reactivation in shales. *Journal of Geophysical Research: Solid Earth*, 120(11): 7729–7748, Nov. 2015b. doi: 10.1002/2015jb012158.

Guglielmi, Y., Cook, P., Soom, F., Schoenball, M., Dobson, P., and Kneafsey, T. In Situ Continuous Monitoring of Borehole Displacements Induced by Stimulated Hydrofracture Growth. *Geophysical Research Letters*, 48(4), Feb. 2021. doi: 10.1029/2020gl090782.

Gulia, L. and Wiemer, S. Real-time discrimination of earthquake foreshocks and aftershocks. *Nature*, 574(7777):193–199, Oct. 2019. doi: 10.1038/s41586-019-1606-4.

Gulia, L., Tormann, T., Wiemer, S., Herrmann, M., and Seif, S. Short-term probabilistic earthquake risk assessment considering time-dependent b values. *Geophysical Research Letters*, 43 (3):1100–1108, Feb. 2016. doi: 10.1002/2015gl066686.

Hamdi, P., Achtziger, P., Dickmann, J., Kruszewski, M., Rinaldi, A. P., Villiger, L., Shakas, A., Perras, M., Bahrani, N., Jiang, D., Amann, F., and Wiemer, S. Progressive Excavation Disturbance Zone Evolution During and Post Mine-By Tunneling (PRECODE) – Insight into a New Underground Research Laboratory for Crystalline Rocks in the BedrettoLab. In *58th U.S. Rock Mechanics/Geomechanics Symposium*, ARMA24. ARMA, June 2024. doi: 10.56952/arma-2024-0543.

Hamdi, P., Ufrecht, S., Achtziger-Zupančič, P., Bröker, K., Ma, X., and Amann, F. Understanding the Regional Stress in Active Tectonic Regime Using 3D Numerical Modeling, Case Study of BedrettoLab, Switzerland. *Rock Mechanics and Rock Engineering*, 58(11):12187–12206, July 2025. doi: 10.1007/s00603-025-04740-0.

Heesakkers, V., Murphy, S., Lockner, D. A., and Reches, Z. Earthquake Rupture at Focal Depth, Part II: Mechanics of the 2004 M2.2 Earthquake Along the Pretorius Fault, TauTona Mine, South Africa. *Pure and Applied Geophysics*, 168(12):2427–2449, Aug. 2011. doi: 10.1007/s00024-011-0355-6.

Hunter, J. D. Matplotlib: A 2D Graphics Environment. *Computing in Science & Engineering*, 9(3):90–95, 2007. doi: 10.1109/mcse.2007.55.

Ide, S., Beroza, G. C., Shelly, D. R., and Uchide, T. A scaling law for slow earthquakes. *Nature*, 447(7140):76–79, May 2007. doi: 10.1038/nature05780.

Ishida, T., Fujito, W., Yamashita, H., Naoi, M., Fuji, H., Suzuki, K., and Matsui, H. Crack Expansion and Fracturing Mode of

Hydraulic Refracturing from Acoustic Emission Monitoring in a Small-Scale Field Experiment. *Rock Mechanics and Rock Engineering*, 52(2):543–553, Jan. 2019. doi: 10.1007/s00603-018-1697-5.

Ito, Y., Obara, K., Shiomi, K., Sekine, S., and Hirose, H. Slow Earthquakes Coincident with Episodic Tremors and Slow Slip Events. *Science*, 315(5811):503–506, Jan. 2007. doi: 10.1126/science.1134454.

Kammer, D. S., McLaskey, G. C., Abercrombie, R. E., Ampuero, J.-P., Cattania, C., Cocco, M., Dal Zilio, L., Dresen, G., Gabriel, A.-A., Ke, C.-Y., Marone, C., Selvadurai, P. A., and Tinti, E. Earthquake energy dissipation in a fracture mechanics framework. *Nature Communications*, 15(1), June 2024. doi: 10.1038/s41467-024-47970-6.

Kaneko, Y. and Ampuero, J.-P. A mechanism for preseismic steady rupture fronts observed in laboratory experiments: MODELING PRESEISMIC STEADY RUPTURE. *Geophysical Research Letters*, 38(21), Nov. 2011. doi: 10.1029/2011gl049953.

Kaneko, Y., Avouac, J.-P., and Lapusta, N. Towards inferring earthquake patterns from geodetic observations of interseismic coupling. *Nature Geoscience*, 3(5):363–369, Apr. 2010. doi: 10.1038/ngeo843.

Kato, A. and Ben-Zion, Y. The generation of large earthquakes. *Nature Reviews Earth & Environment*, 2(1):26–39, Nov. 2020. doi: 10.1038/s43017-020-00108-w.

Kato, A. and Ben-Zion, Y. Publisher Correction: The generation of large earthquakes. *Nature Reviews Earth & Environment*, 2(2): 160–160, Jan. 2021. doi: 10.1038/s43017-021-00145-z.

Kirkpatrick, J. D. and Brodsky, E. E. Slickenline orientations as a record of fault rock rheology. *Earth and Planetary Science Letters*, 408:24–34, Dec. 2014. doi: 10.1016/j.epsl.2014.09.040.

Kozłowska, M., Orlecka-Sikora, B., Kwiatek, G., Boettcher, M. S., and Dresen, G. Nanoseismicity and picoseismicity rate changes from static stress triggering caused by a Mw 2.2 earthquake in Mponeng gold mine, South Africa. *Journal of Geophysical Research: Solid Earth*, 120(1):290–307, Jan. 2015. doi: 10.1002/2014jb011410.

Krietsch, H., Villiger, L., Doetsch, J., Gischig, V., Evans, K. F., Brixel, B., Jalali, M. R., Loew, S., Giardini, D., and Amann, F. Changing Flow Paths Caused by Simultaneous Shearing and Fracturing Observed During Hydraulic Stimulation. *Geophysical Research Letters*, 47(3), Feb. 2020. doi: 10.1029/2019gl086135.

Kurzon, I., Lyakhovsky, V., and Ben-Zion, Y. Dynamic Rupture and Seismic Radiation in a Damage–Breakage Rheology Model. *Pure and Applied Geophysics*, 176(3):1003–1020, Dec. 2018. doi: 10.1007/s00024-018-2060-1.

Kurzon, I., Lyakhovsky, V., and Ben-Zion, Y. Earthquake source properties from analysis of dynamic ruptures and far-field seismic waves in a damage-breakage model. *Geophysical Journal International*, 224(3):1793–1810, Oct. 2020. doi: 10.1093/gji/ggaa509.

Kwiatek, G., Martínez-Garzón, P., Plenkers, K., Leonhardt, M., Zang, A., von Specht, S., Dresen, G., and Bohnhoff, M. Insights Into Complex Subdecimeter Fracturing Processes Occurring During a Water Injection Experiment at Depth in Äspö Hard Rock Laboratory, Sweden. *Journal of Geophysical Research: Solid Earth*, 123(8):6616–6635, Aug. 2018. doi: 10.1029/2017jb014715.

Kwiatek, G., Saarno, T., Ader, T., Bluemle, F., Bohnhoff, M., Chendorain, M., Dresen, G., Heikkinen, P., Kukkonen, I., Leary, P., Leonhardt, M., Malin, P., Martínez-Garzón, P., Passmore, K., Passmore, P., Valenzuela, S., and Wollin, C. Controlling fluid-induced seismicity during a 6.1-km-deep geothermal stimulation in Finland. *Science Advances*, 5(5), May 2019. doi: 10.1126/sciadv.aav7224.

Langenbruch, C. and Zoback, M. D. How will induced seismicity in Oklahoma respond to decreased saltwater injection rates? *Science Advances*, 2(11), Nov. 2016. doi: 10.1126/sciadv.1601542.

Larochelle, S., Lapusta, N., Ampuero, J., and Cappa, F. Constraining Fault Friction and Stability With Fluid-Injection Field Experiments. *Geophysical Research Letters*, 48(10), May 2021. doi: 10.1029/2020gl091188.

Latour, S., Schubnel, A., Nielsen, S., Madariaga, R., and Vinciguerra, S. Characterization of nucleation during laboratory earthquakes. *Geophysical Research Letters*, 40(19):5064–5069, Oct. 2013. doi: 10.1002/grl.50974.

Leeman, J. R., Saffer, D. M., Scuderi, M. M., and Marone, C. Laboratory observations of slow earthquakes and the spectrum of tectonic fault slip modes. *Nature Communications*, 7(1), Mar. 2016. doi: 10.1038/ncomms11104.

Lockner, D. The role of acoustic emission in the study of rock fracture. *International Journal of Rock Mechanics and Mining Sciences & Geomechanics Abstracts*, 30(7):883–899, Dec. 1993. doi: 10.1016/0148-9062(93)90041-b.

Lockner, D. A. and Byerlee, J. D. Dilatancy in hydraulically isolated faults and the suppression of instability. *Geophysical Research Letters*, 21(22):2353–2356, Nov. 1994. doi: 10.1029/94gl02366.

Lockner, D. A., Byerlee, J. D., Kuksenko, V., Ponomarev, A., and Sidorin, A. Quasi-static fault growth and shear fracture energy in granite. *Nature*, 350(6313):39–42, Mar. 1991. doi: 10.1038/350039a0.

Lu, X., Lapusta, N., and Rosakis, A. J. Pulse-like and crack-like ruptures in experiments mimicking crustal earthquakes. *Proceedings of the National Academy of Sciences*, 104(48):18931–18936, Nov. 2007. doi: 10.1073/pnas.0704268104.

Ma, X., Hertrich, M., Amann, F., Bröker, K., Gholizadeh Doonechaly, N., Gischig, V., Hochreutener, R., Kästli, P., Krietsch, H., Marti, M., Nägeli, B., Nejati, M., Obermann, A., Plenkers, K., Rinaldi, A. P., Shakas, A., Villiger, L., Wenning, Q., Zappone, A., Bethmann, F., Castilla, R., Seberto, F., Meier, P., Driesner, T., Loew, S., Maurer, H., Saar, M. O., Wiemer, S., and Giardini, D. Multi-disciplinary characterizations of the BedrettoLab – a new underground geoscience research facility. *Solid Earth*, 13(2):301–322, Feb. 2022. doi: 10.5194/se-13-301-2022.

Mai, P. M., Galis, M., Thingbaijam, K. K. S., Vyas, J. C., and Dunham, E. M. Accounting for Fault Roughness in Pseudo-Dynamic Ground-Motion Simulations. *Pure and Applied Geophysics*, 174 (9):3419–3450, Apr. 2017. doi: 10.1007/s00024-017-1536-8.

Main, I. G., Meredith, P. G., and Sammonds, P. R. Temporal variations in seismic event rate and b-values from stress corrosion constitutive laws. *Tectonophysics*, 211(1–4):233–246, Sept. 1992. doi: 10.1016/0040-1951(92)90061-a.

Marone, C. Laboratory-derived Friction Laws and their Application to Seismic Faulting. *Annual Review of Earth and Planetary Sciences*, 26(1):643–696, May 1998. doi: 10.1146/annurev.earth.26.1.643.

Martínez-Garzón, P. and Poli, P. Cascade and pre-slip models oversimplify the complexity of earthquake preparation in nature. *Communications Earth & Environment*, 5(1), Mar. 2024. doi: 10.1038/s43247-024-01285-y.

McGarr, A. Seismic moments and volume changes. *Journal of Geophysical Research*, 81(8):1487–1494, Mar. 1976. doi: 10.1029/jb081i008p01487.

McGarr, A. Maximum magnitude earthquakes induced by fluid injection: Limits on fluid injection earthquakes. *Journal of Geophysical Research: Solid Earth*, 119(2):1008–1019, Feb. 2014. doi: 10.1002/2013jb010597.

McGuire, J. J. and Kaneko, Y. Directly estimating earthquake

rupture area using second moments to reduce the uncertainty in stress drop. *Geophysical Journal International*, 214(3): 2224–2235, June 2018. doi: 10.1093/gji/ggy201.

McLaskey, G. C. Earthquake Initiation From Laboratory Observations and Implications for Foreshocks. *Journal of Geophysical Research: Solid Earth*, 124(12):12882–12904, Dec. 2019. doi: 10.1029/2019jb018363.

Meier, M., Heaton, T., and Clinton, J. Evidence for universal earthquake rupture initiation behavior. *Geophysical Research Letters*, 43(15):7991–7996, Aug. 2016. doi: 10.1002/2016gl070081.

Meier, M.-A., Ampuero, J. P., and Heaton, T. H. The hidden simplicity of subduction megathrust earthquakes. *Science*, 357(6357): 1277–1281, Sept. 2017. doi: 10.1126/science.aan5643.

Meier, M.-A., Ampuero, J.-P., Cochran, E., and Page, M. Apparent earthquake rupture predictability. *Geophysical Journal International*, 225(1):657–663, Dec. 2020. doi: 10.1093/gji/ggaa610.

Meier, M.-A., Gischig, V., Rinaldi, A., Jalali, M., Supino, M., Mosconi, F., Villiger, L., Selvadurai, P., Spagnuolo, E., Tinti, E., Dal Zilio, L., Zappone, A., Pozzi, G., Mesimeri, M., Scarabello, L., Hertrich, M., Amann, F., Cocco, M., Wiemer, S., and Giardini, D. An Induced Mw -0.4 Earthquake Under a Microscope at the BedrettoLab. Mar. 2025. doi: 10.5194/egusphere-egu25-17272.

Mesimeri, M., Scarabello, L., Zimmermann, E., Haag, T., Zylis, E., Villiger, L., Kaestli, P., Meier, M.-A., Rinaldi, A. P., Obermann, A., Hertrich, M., Clinton, J., Giardini, D., and Wiemer, S. Multiscale Seismic Monitoring in the Bedretto Underground Laboratory for Geosciences and Geoenergies (BULGG). *Seismological Research Letters*, 96(1):182–191, July 2024. doi: 10.1785/0220240128.

Meyer, G. G., Giorgetti, C., Guérin-Marthe, S., and Violay, M. Off-fault deformation feedback and strain localization precursor during laboratory earthquakes. *Communications Earth & Environment*, 5(1), Oct. 2024. doi: 10.1038/s43247-024-01756-2.

Mignan, A., Ouillon, G., Sornette, D., and Freund, F. Global Earthquake Forecasting System (GEFS): The challenges ahead. *The European Physical Journal Special Topics*, 230(1):473–490, Jan. 2021. doi: 10.1140/epjst/e2020-000261-8.

Moein, M. J. A., Langenbruch, C., Schultz, R., Grigoli, F., Ellsworth, W. L., Wang, R., Rinaldi, A. P., and Shapiro, S. The physical mechanisms of induced earthquakes. *Nature Reviews Earth & Environment*, 4(12):847–863, Dec. 2023. doi: 10.1038/s43017-023-00497-8.

Mosconi, F., Tinti, E., Casarotti, E., Gabriel, A., Rinaldi, A. P., Dal Zilio, L., and Cocco, M. Modeling the 3D Dynamic Rupture of Microearthquakes Induced by Fluid Injection. *Journal of Geophysical Research: Solid Earth*, 130(3), Mar. 2025. doi: 10.1029/2024jb029621.

Naoi, M., Ogasawara, H., Takeuchi, J., Yamamoto, A., Shimoda, N., Morishita, K., Ishii, H., Nakao, S., van Aswegen, G., Mendecki, A. J., Lenegan, P., Ebrahim-Trollope, R., and Iio, Y. Small slow-strain steps and their forerunners observed in gold mine in South Africa. *Geophysical Research Letters*, 33(12), June 2006. doi: 10.1029/2006gl026507.

Naoi, M., Nakatani, M., Yabe, Y., Kwiatek, G., Igarashi, T., and Plenkers, K. Twenty Thousand Aftershocks of a Very Small (M 2) Earthquake and Their Relation to the Mainshock Rupture and Geological Structures. *Bulletin of the Seismological Society of America*, 101(5):2399–2407, Sept. 2011. doi: 10.1785/0120100346.

Obara, K. Nonvolcanic Deep Tremor Associated with Subduction in Southwest Japan. *Science*, 296(5573):1679–1681, May 2002. doi: 10.1126/science.1070378.

Obara, K. and Kato, A. Connecting slow earthquakes to huge earthquakes. *Science*, 353(6296):253–257, July 2016. doi: 10.1126/science.aaf1512.

Obermann, A., Rosskopf, M., Durand, V., Plenkers, K., Bröker, K., Rinaldi, A. P., Gholizadeh Doonechaly, N., Gischig, V., Zappone, A., Amann, F., Cocco, M., Hertrich, M., Jalali, M., Junker, J. S., Kästli, P., Ma, X., Maurer, H., Meier, M., Schwarz, M., Selvadurai, P., Villiger, L., Wiemer, S., Dal Zilio, L., and Giardini, D. Seismic Response of Hectometer-Scale Fracture Systems to Hydraulic Stimulation in the Bedretto Underground Laboratory, Switzerland. *Journal of Geophysical Research: Solid Earth*, 129(11), Nov. 2024. doi: 10.1029/2024jb029836.

Ogasawara, H. *Review of semi-controlled earthquake-generation experiments in South African deep gold mines (1992–2001)*, page 119–150. Routledge, 2002. doi: 10.1201/9780203739990-11.

Ohnaka, M. Earthquake source nucleation: A physical model for short-term precursors. *Tectonophysics*, 211(1–4):149–178, Sept. 1992. doi: 10.1016/0040-1951(92)90057-d.

Ohnaka, M. A constitutive scaling law and a unified comprehension for frictional slip failure, shear fracture of intact rock, and earthquake rupture. *Journal of Geophysical Research: Solid Earth*, 108 (B2), Feb. 2003. doi: 10.1029/2000jb000123.

Osten, J., Schaber, T., Gaus, G., Hamdi, P., Amann, F., and Achtziger-Zupančič, P. A multi-method investigation of the permeability structure of brittle fault zones with ductile precursors in crystalline rock. *Grundwasser*, 29(1):49–61, Jan. 2024. doi: 10.1007/s00767-023-00561-6.

Paterson, M. and Wong, T.-F. *Experimental Rock Deformation—The Brittle Field*. Springer, Berlin / Heidelberg, 2nd edition, 2005.

Plenkers, K., Kwiatek, G., Nakatani, M., and Dresen, G. Observation of Seismic Events with Frequencies f > 25 kHz at Mponeng Deep Gold Mine, South Africa. *Seismological Research Letters*, 81(3): 467–479, May 2010. doi: 10.1785/gssrl.81.3.467.

Plenkers, K., Reinicke, A., Obermann, A., Gholizadeh Doonechaly, N., Krietsch, H., Fechner, T., Hertrich, M., Kontar, K., Maurer, H., Philipp, J., Rinderknecht, B., Volksdorf, M., Giardini, D., and Wiemer, S. Multi-Disciplinary Monitoring Networks for Mesoscale Underground Experiments: Advances in the Bedretto Reservoir Project. *Sensors*, 23(6):3315, Mar. 2023. doi: 10.3390/s23063315.

Pozzi, G., Collettini, C., Scuderi, M. M., Tesei, T., Marone, C., Amodio, A., and Cocco, M. Fabric controls fault stability in serpentinite gouges. *Geophysical Journal International*, 235(2):1778–1797, July 2023. doi: 10.1093/gji/ggad322.

Proctor, B., Lockner, D. A., Kilgore, B. D., Mitchell, T. M., and Beeler, N. M. Direct Evidence for Fluid Pressure, Dilatancy, and Compaction Affecting Slip in Isolated Faults. *Geophysical Research Letters*, 47(16), Aug. 2020. doi: 10.1029/2019gl086767.

Rast, M., Galli, A., Ruh, J. B., Guillong, M., and Madonna, C. Geology along the Bedretto tunnel: kinematic and geochronological constraints on the evolution of the Gotthard Massif (Central Alps). *Swiss Journal of Geosciences*, 115(1), Mar. 2022. doi: 10.1186/s00015-022-00409-w.

Renard, F. and Candela, T. Scaling of Fault Roughness and Implications for Earthquake Mechanics, June 2017. doi: 10.1002/9781119156895.ch10.

Renner, J., Adero, B., Becker, F., Blümle, F., Boese, C., and Cheng, Y. STIMTEC – A mine-scale hydraulic stimulation experi-ment of anisotropic metamorphic rock with evaluation by mine-back drilling. In Ma, X., editor, *Introduction to the special issue: deep underground laboratories (DUL), ARMA Newsletter*. 2021. https://. armarocks.org/wp-content/uploads/2021/01/2021_issue_30_winter.pdf.

Rice, J. R. On the stability of dilatant hardening for saturated rock masses. *Journal of Geophysical Research*, 80(11):1531–1536, Apr. 1975. doi: 10.1029/jb080i011p01531.

Rice, J. R. Spatio-temporal complexity of slip on a fault. *Journal*

of Geophysical Research: Solid Earth, 98(B6):9885–9907, June 1993. doi: 10.1029/93jb00191.

Rice, J. R. and Cocco, M. *Seismic Fault Rheology and Earthquake Dynamics*, page 99–138. The MIT Press, May 2007. doi: 10.7551/mitpress/6703.003.0007.

Ripperger, J., Ampuero, J., Mai, P. M., and Giardini, D. Earthquake source characteristics from dynamic rupture with constrained stochastic fault stress. *Journal of Geophysical Research: Solid Earth*, 112(B4), Apr. 2007. doi: 10.1029/2006jb004515.

Rosenau, M., Corbi, F., and Dominguez, S. Analogue earthquakes and seismic cycles: experimental modelling across timescales. *Solid Earth*, 8(3):597–635, May 2017. doi: 10.5194/se-8-597-2017.

Rosskopf, M., Durand, V., Plenkers, K., Villiger, L., Giardini, D., and Obermann, A. Accuracy of Picoseismic Catalogs in Hectometer-Scale In Situ Experiments. *Seismological Research Letters*, 96(6): 3814–3836, July 2025. doi: 10.1785/0220240399.

Rouet-Leduc, B., Hulbert, C., Lubbers, N., Barros, K., Humphreys, C. J., and Johnson, P. A. Machine Learning Predicts Laboratory Earthquakes. *Geophysical Research Letters*, 44(18):9276–9282, Sept. 2017. doi: 10.1002/2017gl074677.

Rubino, V., Rosakis, A. J., and Lapusta, N. Understanding dynamic friction through spontaneously evolving laboratory earthquakes. *Nature Communications*, 8(1), June 2017. doi: 10.1038/ncomms15991.

Ruina, A. Slip instability and state variable friction laws. *Journal of Geophysical Research: Solid Earth*, 88(B12):10359–10370, Dec. 1983. doi: 10.1029/jb088ib12p10359.

Saffer, D. M. and Tobin, H. J. Hydrogeology and Mechanics of Subduction Zone Forearcs: Fluid Flow and Pore Pressure. *Annual Review of Earth and Planetary Sciences*, 39(1):157–186, May 2011. doi: 10.1146/annurev-earth-040610-133408.

Sagy, A., Brodsky, E. E., and Axen, G. J. Evolution of fault-surface roughness with slip. *Geology*, 35(3):283, 2007. doi: 10.1130/g23235a.1.

Salazar Vásquez, A., Selvadurai, P., Bianchi, P., Madonna, C., Germanovich, L., Puzrin, A., Wiemer, S., Giardini, D., and Rabaiotti, C. Aseismic strain localization prior to failure and associated seismicity in crystalline rock. *Scientific Reports*, 14, 2024. doi: 10.1038/s41598-024-75942-9.

Scholz, C. H. *The Mechanics of Earthquakes and Faulting*. Cambridge University Press, Dec. 2018. doi: 10.1017/9781316681473.

Scholz, C. H., Sykes, L. R., and Aggarwal, Y. P. Earthquake Prediction: A Physical Basis. *Science*, 181(4102):803–810, Aug. 1973. doi: 10.1126/science.181.4102.803.

Schultz, R. Reining-In the Spring-Slider With Reinforcement Learning. *Journal of Geophysical Research: Solid Earth*, 130(3), Mar. 2025. doi: 10.1029/2024jb029697.

Schultz, R., Atkinson, G., Eaton, D. W., Gu, Y. J., and Kao, H. Hydraulic fracturing volume is associated with induced earthquake productivity in the Duvernay play. *Science*, 359(6373): 304–308, Jan. 2018. doi: 10.1126/science.aao0159.

Schultz, R., Lanza, F., Dyer, B., Karvounis, D., Fiori, R., Shi, P., Ritz, V., Villiger, L., Meier, P., and Wiemer, S. The bound growth of induced earthquakes could de-risk hydraulic fracturing. *Communications Earth & Environment*, 6(1), Nov. 2025. doi: 10.1038/s43247-025-02881-2.

Schwarz, M. L., Maurer, H., Obermann, A. C., Selvadurai, P. A., Shakas, A., Wiemer, S., and Giardini, D. New insights on the fault structure of a geothermal testbed and the associated seismicity based on active seismic tomography. Mar. 2025. doi: 10.5194/egusphere-2025-1094.

Scuderi, M. M., Carpenter, B. M., Johnson, P. A., and Marone, C. Poromechanics of stick-slip frictional sliding and strength recovery on tectonic faults. *Journal of Geophysical Research: Solid Earth*, 120(10):6895–6912, Oct. 2015. doi: 10.1002/2015jb011983.

Segall, P. and Rice, J. R. Dilatancy, compaction, and slip instability of a fluid-infiltrated fault. *Journal of Geophysical Research: Solid Earth*, 100(B11):22155–22171, Nov. 1995. doi: 10.1029/95jb02403.

Selvadurai, P. and Glaser, S. Asperity generation and its relationship to seismicity on a planar fault: a laboratory simulation. *Geophysical Journal International*, 208(2):1009–1025, Nov. 2016. doi: 10.1093/gji/ggw439.

Selvadurai, P., Galvez, P., Mai, P., and Glaser, S. Modeling frictional precursory phenomena using a wear-based rate- and state-dependent friction model in the laboratory. *Tectonophysics*, 847:229689, Jan. 2023. doi: 10.1016/j.tecto.2022.229689.

Selvadurai, P. A. Laboratory Insight Into Seismic Estimates of Energy Partitioning During Dynamic Rupture: An Observable Scaling Breakdown. *Journal of Geophysical Research: Solid Earth*, 124(11):11350–11379, Nov. 2019. doi: 10.1029/2018jb017194.

Selvadurai, P. A. and Glaser, S. D. Laboratory-developed contact models controlling instability on frictional faults. *Journal of Geophysical Research: Solid Earth*, 120(6):4208–4236, June 2015. doi: 10.1002/2014jb011690.

Selvadurai, P. A. and Selvadurai, A. P. S. On the Influence of a Dilatant Asperity Patch on the Seismic Moment. *Journal of Elasticity*, 157(3), May 2025. doi: 10.1007/s10659-025-10135-7.

Shipton, Z. K., Soden, A. M., Kirkpatrick, J. D., Bright, A. M., and Lunn, R. J. *How thick is a fault? Fault displacement-thickness scaling revisited*, page 193–198. American Geophysical Union, 2006. doi: 10.1029/170gm19.

Socquet, A., Valdes, J. P., Jara, J., Cotton, F., Walpersdorf, A., Cotte, N., Specht, S., Ortega-Culaciati, F., Carrizo, D., and Norabuena, E. An 8 month slow slip event triggers progressive nucleation of the 2014 Chile megathrust. *Geophysical Research Letters*, 44(9): 4046–4053, May 2017. doi: 10.1002/2017gl073023.

Spagnuolo, E., Cornelio, C., Aretusini, S., Pozzi, G., Cocco, M., Selvadurai, P., and Di Stefano, G. A novel apparatus to study the mechano-chemical processes active during the nucleation and propagation of earthquakes (MEERA). May 2023. doi: 10.5194/egusphere-egu23-8807.

Supino, M., Festa, G., and Zollo, A. A probabilistic method for the estimation of earthquake source parameters from spectral inversion: application to the 2016–2017 Central Italy seismic sequence. *Geophysical Journal International*, 218(2):988–1007, May 2019. doi: 10.1093/gji/ggz206.

Swiss Seismological Service (SED) at ETH Zurich. Bedretto Underground Laboratory for Geosciences and Geoenergies (BULGG) Seismic Network, Switzerland, 2018. doi: 10.12686/SED/NETWORKS/8R.

Torabi, A. and Berg, S. S. Scaling of fault attributes: A review. *Marine and Petroleum Geology*, 28(8):1444–1460, Aug. 2011. doi: 10.1016/j.marpetgeo.2011.04.003.

Tormann, T., Wiemer, S., and Mignan, A. Systematic survey of high-resolutionbvalue imaging along Californian faults: Inference on asperities. *Journal of Geophysical Research: Solid Earth*, 119(3): 2029–2054, Mar. 2014. doi: 10.1002/2013jb010867.

Tormann, T., Enescu, B., Woessner, J., and Wiemer, S. Randomness of megathrust earthquakes implied by rapid stress recovery after the Japan earthquake. *Nature Geoscience*, 8(2):152–158, Feb. 2015. doi: 10.1038/ngeo2343.

Tullis, T. E. Rock friction and its implications for earthquake pre-

diction examined via models of Parkfield earthquakes. *Proceedings of the National Academy of Sciences*, 93(9):3803–3810, Apr. 1996. doi: 10.1073/pnas.93.9.3803.

van der Elst, N. J., Page, M. T., Weiser, D. A., Goebel, T. H., and Hosseini, S. M. Induced earthquake magnitudes are as large as (statistically) expected. *Journal of Geophysical Research: Solid Earth*, 121(6):4575–4590, June 2016. doi: 10.1002/2016jb012818.

Volpe, G., Pozzi, G., Collettini, C., Spagnuolo, E., Achtziger-Zupančič, P., Zappone, A., Aldega, L., Meier, M., Giardini, D., and Cocco, M. Laboratory simulation of fault reactivation by fluid injection and implications for induced seismicity at the BedrettoLab, Swiss Alps. *Tectonophysics*, 862:229987, Sept. 2023. doi: 10.1016/j.tecto.2023.229987.

Wang, L., Kwiatek, G., Renard, F., Guérin-Marthe, S., Rybacki, E., Bohnhoff, M., Naumann, M., and Dresen, G. Fault roughness controls injection-induced seismicity. *Proceedings of the National Academy of Sciences*, 121(3), Jan. 2024. doi: 10.1073/pnas.2310039121.

Weingarten, M., Ge, S., Godt, J. W., Bekins, B. A., and Rubinstein, J. L. High-rate injection is associated with the increase in U.S. mid-continent seismicity. *Science*, 348(6241):1336–1340, June 2015. doi: 10.1126/science.aab1345.

Wu, B. and Barbot, S. Evolution of the real area of contact during laboratory earthquakes. *Proceedings of the National Academy of Sciences*, 122(23), June 2025. doi: 10.1073/pnas.2410496122.

Xu, S., Fukuyama, E., Yamashita, F., Kawakata, H., Mizoguchi, K., and Takizawa, S. Fault strength and rupture process controlled by fault surface topography. *Nature Geoscience*, 16(1):94–100, Jan. 2023. doi: 10.1038/s41561-022-01093-z.

Yabe, Y., Nakatani, M., Naoi, M., Philipp, J., Janssen, C., Watanabe, T., Katsura, T., Kawakata, H., Georg, D., and Ogasawara, H. Nucleation process of an M2 earthquake in a deep gold mine in South Africa inferred from on-fault foreshock activity. *Journal of Geophysical Research: Solid Earth*, 120(8):5574–5594, Aug. 2015. doi: 10.1002/2014jb011680.

Yamada, T., Mori, J. J., Ide, S., Abercrombie, R. E., Kawakata, H., Nakatani, M., Iio, Y., and Ogasawara, H. Stress drops and radiated seismic energies of microearthquakes in a South African gold mine. *Journal of Geophysical Research: Solid Earth*, 112 (B3), Mar. 2007. doi: 10.1029/2006jb004553.

Ye, Z. and Ghassemi, A. Injection-Induced Shear Slip and Permeability Enhancement in Granite Fractures. *Journal of Geophysical Research: Solid Earth*, 123(10):9009–9032, Oct. 2018. doi: 10.1029/2018jb016045.

Zang, A., Stephansson, O., Stenberg, L., Plenkers, K., Specht, S., Milkereit, C., Schill, E., Kwiatek, G., Dresen, G., Zimmermann, G., Dahm, T., and Weber, M. Hydraulic fracture monitoring in hard rock at 410 m depth with an advanced fluid-injection protocol and extensive sensor array. *Geophysical Journal International*, 208(2):790–813, Nov. 2016. doi: 10.1093/gji/ggw430.

Zappone, A., Rinaldi, A. P., Grab, M., Wenning, Q. C., Roques, C., Madonna, C., Obermann, A. C., Bernasconi, S. M., Brennwald, M. S., Kipfer, R., Soom, F., Cook, P., Guglielmi, Y., Nussbaum, C., Giardini, D., Mazzotti, M., and Wiemer, S. Fault sealing and caprock integrity for CO 2 storage: an in situ injection experiment. *Solid Earth*, 12(2):319–343, Feb. 2021. doi: 10.5194/se-12-319-2021.

Zhong, Z., Song, Z., Li, B., Elsworth, D., Hu, Y., Zhang, F., and Chen, Z. Controls of Gouge Heterogeneity on Cyclic Reactivation of Fault-Valve Systems. *Geophysical Research Letters*, 52(14), July 2025. doi: 10.1029/2025gl115092.

Ziegler, M., Reiter, K., Heidbach, O., Zang, A., Kwiatek, G., Stromeyer, D., Dahm, T., Dresen, G., and Hofmann, G. Mining-Induced Stress Transfer and Its Relation to a Mw 1.9 Seismic Event in an Ultra-deep South African Gold Mine. *Pure and Applied Geophysics*, 172(10):2557–2570, Feb. 2015. doi: 10.1007/s00024-015-1033-x.